JBC ARTICLE

Author's Choice

# Assessment of $H_2S$ *in vivo* using the newly developed mitochondria-targeted mass spectrometry probe MitoA

Received for publication, March 6, 2017, and in revised form, March 17, 2017 Published, Papers in Press, March 20, 2017, DOI 10.1074/jbc.M117.784678

**Sabine Arndt[‡], Carlos D. Baeza-Garza[§], Angela Logan[‡], Tiziana Rosa[¶], Rudolf Wedmann[‖], Tracy A. Prime[‡], Jack L. Martin[**], Kourosh Saeb-Parsy[**], Thomas Krieg[¶], Milos R. Filipovic[‖‡‡1], Richard C. Hartley[§2], and Michael P. Murphy[‡3]**

*From the [‡]MRC Mitochondrial Biology Unit, University of Cambridge, Hills Road, Cambridge CB2 0XY, United Kingdom, the [§]WestCHEM School of Chemistry, University of Glasgow, Glasgow G12 8QQ, United Kingdom, the [¶]Department of Medicine, University of Cambridge, Biomedical Campus, Cambridge, CB2 2QQ, United Kingdom, the [‖]Department of Chemistry and Pharmacy, Friedrich-Alexander University of Erlangen-Nuremberg, Egerlandstrasse,1, 91058 Erlangen, Germany, the [‡‡]University of Bordeaux, IBGC, UMR 5095, F-33077 Bordeaux, France, and the [**]Department of Surgery and Cambridge NIHR Biomedical Research Centre, Biomedical Campus, University of Cambridge, Cambridge CB2 2QQ, United Kingdom*

Edited by Ruma Banerjee

**Hydrogen sulfide ($H_2S$) is produced endogenously *in vivo* and has multiple effects on signaling pathways and cell function. Mitochondria can be both an $H_2S$ source and sink, and many of the biological effects of $H_2S$ relate to its interactions with mitochondria. However, the significance of mitochondrial $H_2S$ is uncertain, in part due to the difficulty of assessing changes in its concentration *in vivo*. Although a number of fluorescent $H_2S$ probes have been developed these are best suited to cells in culture and cannot be used *in vivo*. To address this unmet need we have developed a mitochondria-targeted $H_2S$ probe, MitoA, which can be used to assess relative changes in mitochondrial $H_2S$ levels *in vivo*. MitoA comprises a lipophilic triphenylphosphonium (TPP) cation coupled to an aryl azide. The TPP cation leads to the accumulation of MitoA inside mitochondria within tissues *in vivo*. There, the aryl azido group reacts with $H_2S$ to form an aryl amine (MitoN). The extent of conversion of MitoA to MitoN thus gives an indication of the levels of mitochondrial $H_2S$ *in vivo*. Both compounds can be detected sensitively by liquid chromatography tandem mass spectrometry (LC-MS/MS) analysis of the tissues, and quantified relative to deuterated internal standards. Here we describe the synthesis and characterization of MitoA and show that it can be used to assess changes in mitochondrial $H_2S$ levels *in vivo*. As a proof of principle we used MitoA to show that $H_2S$ levels increase *in vivo* during myocardial ischemia.**

There is considerable interest in the biological roles of hydrogen sulfide ($H_2S$), both as an endogenously produced modulator of mammalian metabolism and for its potential biomedical effects when generated pharmacologically (1–3). Changes in endogenous $H_2S$ levels have been claimed to impact on a diverse range of physiological processes, including neuronal function, blood pressure, angiogenesis, oxygen sensing, inflammation, and mitochondrial energy production (4–16), and exposure to $H_2S$ can induce a suspended animation-like state in mice (17), but not in larger animals (18, 19).

Within mammals there are three main enzymatic sources of $H_2S$: cystathionine $\beta$-synthase and cystathionine $\gamma$-lyase in the cytosol, and mitochondrial 3-mercaptopyruvate sulfurtransferase in conjunction with cysteine aminotransferase (Fig. 1*A*) (20). Once generated, $H_2S$ can be oxidized by sulfide:quinone oxidoreductase (SQR)[4] in the mitochondrial inner membrane, passing electrons to the CoQ pool, and in parallel generating glutathione persulfide in the matrix, which is further metabolized to thiosulfate/sulfite/sulfate in the mitochondrial matrix and intermembrane space (21, 22) (Fig. 1*A*).

The biological activity of $H_2S$ arises from four interrelated processes: protein persulfidation, binding to metalloprotein centers (most notably, inhibition of cytochrome oxidase), interaction with NO signaling pathways, and as an antioxidant (14, 20). Protein persulfidation is a recently emerging mode of reversible posttranslational modification (PTM) of protein thiols in which $H_2S$ can react with a disulfide or a sulfenic acid, but not unmodified protein thiols, to form a persulfidated protein thiol (PrSSH), which can be reduced back to a thiol by the glutathione or thioredoxin systems (23, 24). This reversible PTM can in principle modify protein activity in a similar way to other PTMs, or can act as a releasable pool of $H_2S$; however, the extent and physiological significance of protein persulfidation is still emerging. $H_2S$ can also inhibit cytochrome oxidase (25), which is why high concentrations of $H_2S$ are toxic, but whether these interactions with cytochrome oxidase or other heme proteins are of physiological or pharmacological importance is

This work was supported in part by Medical Research Council UK Grant MC_U105663142, Wellcome Trust Investigator award 110159/Z/15/Z (to M. P. M.), Biotechnology and Biological Sciences Research Council Grant BB/I012826/1, Wellcome Trust Investigator award 110158/Z/15/Z (to R. C. H.), and a Consejo Nacional de Ciencia y Tecnología studentship (to C. B.-G.). The authors declare that they have no conflicts of interest with the contents of this article.



This article contains supplemental Figs. S1–S5.

[1] Supported by a CNRS/INSERM Atip-Avenir grant.

[2] To whom correspondence may be addressed. Tel.: 44-141-330-4398; E-mail: Richard.Hartley@glasgow.ac.uk.

[3] To whom correspondence may be addressed. Tel.: 44-1223-252-900; E-mail: mpm@mrc-mbu.cam.ac.uk.

[4] The abbreviations used are: SQR, sulfide:quinone oxidoreductase; PTM, posttranslational modification; NAP, *N*-acetylpenicillamine; IS, internal standards; TPP, triphenylphosphonium; LAD model, left anterior descending model; ACN, acetonitrile; FA, formic acid.

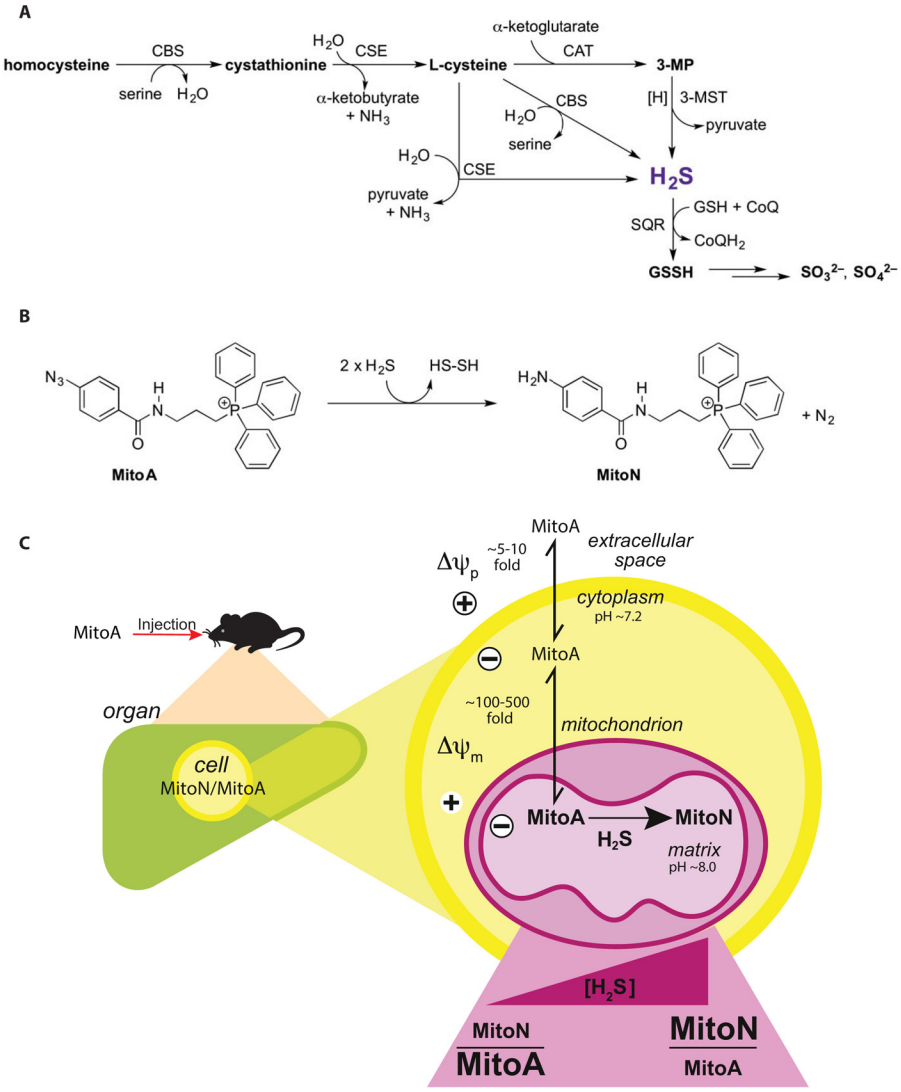


**Figure 1. Overview of endogenous $H_2S$ production and rationale for its detection by MitoA.** *A*, overview of $H_2S$ metabolism (sulfur-containing compounds in bold). *CBS*, cystathionine β-synthase; *CSE*, cystathionine β-lyase; *CAT*, cysteine aminotransferase; *GSSH*, glutathione persulfide; *3-MP*, 3-mercaptopyruvate; *3-MST*, 3-mercaptopyruvate sulfurtransferase. *B*, reaction of MitoA with $H_2S$ to form MitoN. *C*, model of uptake of MitoA into mitochondria *in vivo*, followed by its conversion to MitoN upon reaction with $H_2S$. The subsequent extraction of MitoA and MitoN from the tissue and analysis by LC-MS/MS enables changes in the levels of $H_2S$ *in vivo* to be inferred.

unclear. $H_2S$ signaling is intimately interwoven with that of NO, due to the formation of HSNO and other intermediates, and it is likely that protein modification by persulfidation and *S*-nitrosation are facets of a general signaling pathway (26, 27). Finally, $H_2S$ may also contribute to antioxidant defenses, by reacting directly with oxidants, or indirectly through its interactions with protein thiols (20, 28).

Abnormal $H_2S$ levels have been reported in a range of pathologies including Down syndrome (29), diabetes (30), liver cirrhosis, and in ethylmalonic acid encephalopathy, which occurs due to mutation to *ETHE1* (31). However, the factors that modify $H_2S$ levels *in vivo* under normal and pathological conditions are obscure. In addition, the contribution of $H_2S$ generation to the efficacy of pharmacological agents that release $H_2S$ is uncertain. Therefore, understanding how the levels of $H_2S$ change *in vivo* is vital to understanding its roles in physiology, pathology, and pharmacology.

There are a number of methods to assess $H_2S$ in cells using fluorescent probes that allow real-time detection of changes in $H_2S$ levels (32–40). Although these methods can be applied to the surfaces of animals (41), and to blood *ex vivo* (42), they cannot be used in whole animals *in vivo*. Consequently, there are considerable uncertainties about how $H_2S$ tissue levels change in response to physiological, pathological, or pharmacological events. These uncertainties are a major impediment to better understanding the biological roles of $H_2S$ and its downstream targets.

To overcome this obstacle, we have developed MitoA, a mitochondria-targeted mass spectrometry probe for $H_2S$ detection *in vivo* (Fig. 1*B*). The probe comprises an $H_2S$-sensitive aryl azide moiety coupled to the lipophilic triphenylphosphonium (TPP) cation (Fig. 1*B*). The TPP cation targets a wide range of bioactive and probe compounds to mitochondria *in vivo* in response to the mitochondrial membrane potential (43, 44), and thus should lead to the rapid uptake of MitoA into

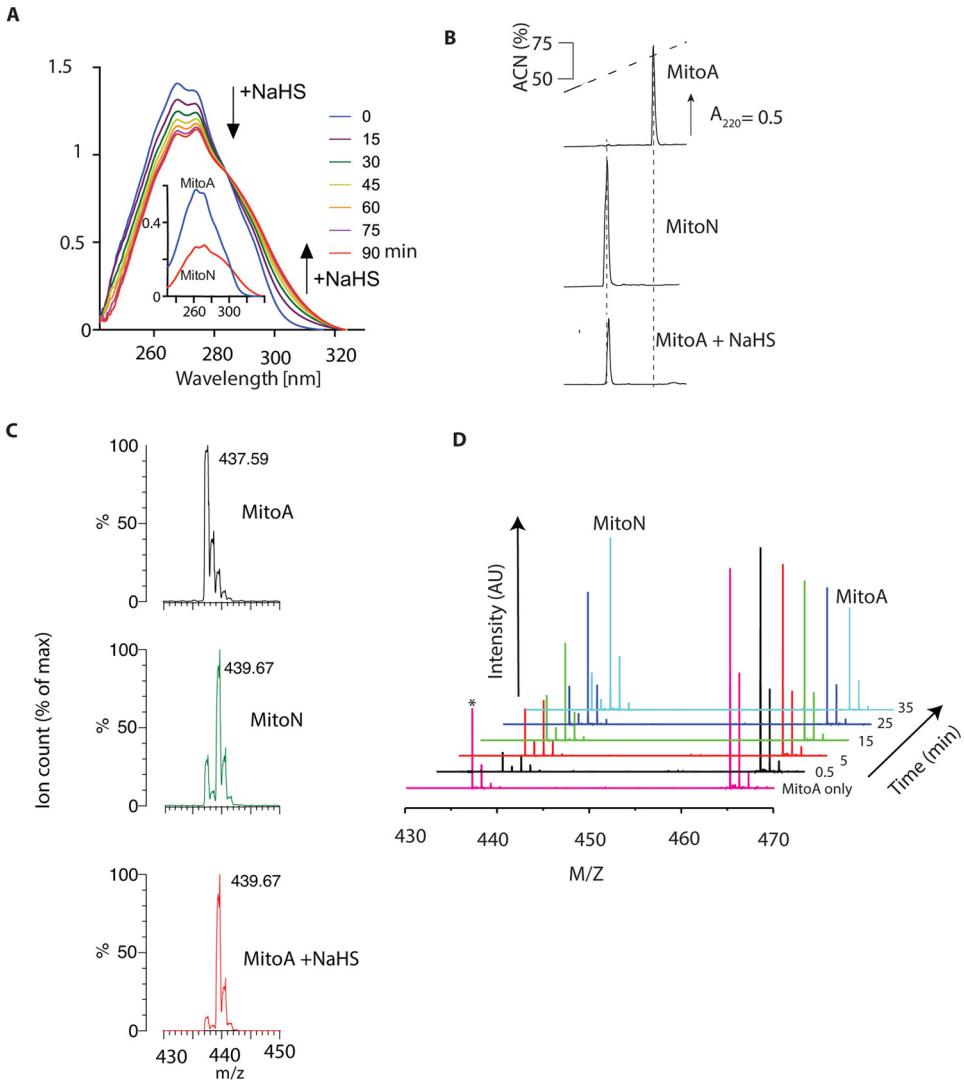


**Figure 2. Reaction of MitoA with $H_2S$ to form MitoN.** *A,* UV-visual absorbance spectra of MitoA reacting with NaHS. MitoA (50 $\mu$M) in KCl buffer was mixed with 5 mM NaHS and spectra were taken every 15 min. The *inset* shows spectra of pure MitoA and MitoN (25 $\mu$M each). *B,* RP-HPLC analysis of MitoA, MitoN, and its reactivity with $H_2S$. Standards of 10 nmol of MitoA (*upper trace*) or MitoN (*middle trace*) were separated by RP-HPLC. For the *lower trace* MitoA (100 $\mu$M) in KCl buffer was incubated overnight with 1 mM NaHS at room temperature. Then 5 nmol eq of starting MitoA was analyzed by RP-HPLC. Spiking the NaHS-treated MitoA with MitoN increased the MitoN peak (data not shown). *C,* mass spectra of MitoA, MitoN, or MitoA incubated overnight with NaHS. Mass spectra were taken of MitoA (100 $\mu$M), MitoN (100 $\mu$M), or MitoA (100 $\mu$M) incubated with 1 mM NaHS in KCl buffer, pH 7.2, overnight at room temperature. Samples were diluted in 20% ACN, 0.1% FA and analyzed within 5 h. Predicted *m/z*: MitoA, $[C_{28}H_{26}N_4OP]^+ = 465.18$; nitrene from neutral loss of $N_2$, $[C_{28}H_{26}N_2OP]^+ = 437.17$; MitoN, $[C_{28}H_{29}N_2OP]^+ = 439.19$. The MS of MitoA incubated at room temperature overnight was the same as that for freshly prepared MitoA (data not shown). *D,* time-resolved analysis of the reaction of MitoA with $H_2S$. MitoA (100 $\mu$M) was mixed with 2.5 mM $H_2S$ in 300 mM ammonium carbonate, pH 7.4, and sprayed continuously over 45 min into an ultra high resolution mass spectrometer (maXis Bruker Daltonics). Spectra at selected time points are shown. *Asterisk* shows the nitrene formed from MitoA by the neutral loss of $N_2$.

mitochondria *in vivo*. Within the mitochondrial matrix the aryl azide moiety is intended to react with $H_2S$ to form the aryl amine, MitoN (Fig. 1*B*). This chemistry is based on that of widely used $H_2S$-sensitive fluorescent probes, which rely on the reaction of a non-fluorescent aryl azide to give a fluorescent aryl amine (33, 37, 45, 46). The reaction occurs by initial nucleophilic attack of $HS^-$ on the electrophilic terminal nitrogen of the aryl azide, followed by a rate-determining reaction with a second $HS^-$, forming $HS_2^-$, $N_2$, and the aryl amine (37) (Fig. 1*B*). Thus, MitoA can be injected into animals and the extent of generation of the exomarker MitoN will depend on the levels of $H_2S$ within mitochondria *in vivo*. Similar exomarker approaches have been used *in vivo* to assess hydrogen peroxide using MitoB (47, 48), and glyoxals through MitoG (49, 50). To analyze MitoA and its conversion to MitoN, both are extracted from animal tissue and then analyzed by LC-MS/MS relative to deuterated internal standards (Fig. 1*C*). Because MitoA is mainly present within mitochondria *in vivo*, it will report on the local concentration of $H_2S$ within mitochondria. However, because $H_2S$ diffuses rapidly across cellular membranes, $H_2S$ levels in the mitochondria are likely to reflect or influence overall changes in $H_2S$ within cells *in vivo*. Here we report the development of MitoA and show that it can be used to assess changes in $H_2S$ *in vivo*.

## Results and discussion

### *Reaction of MitoA with $H_2S$ to form MitoN*

We first determined whether MitoA reacted with $H_2S$ to form MitoN by measuring the effect of $H_2S$ on the UV absorption spectra of MitoA over time (Fig. 2*A*). Addition of NaHS,

**Table 1**

**MitoA (10 $\mu$M) was incubated with each substance for the indicated time and temperature in KCl buffer and analyzed by RP-HPLC**

Dimethyl trisulfide was dissolved in 70% EtOH. For NO, DetaNONOate (50 $\mu$M) was disolved in KCl buffer, which had been deoxygenated by bubbling with argon for 30 min. Superoxide was generated using 5 milliunits/ml of xanthine oxidase and 1 mM hypoxanthine in KCl buffer and its production quantified as the SOD-sensitive reduction of ferricytochrome *c*. Reactivity = (MitoN × 100)/(MitoN + MitoA).

| | Concentration | Incubation condition | Reactivity |
|---|---|---|---|
| | | | % |
| $H_2S$ | 100 $\mu$M | 4 h, RT[a] | 94 |
| Glutathione | 5 mM | 24 h, 37 °C | 7.3 |
| | 5 mM | 4 h, 37 °C | 2.2 |
| | 10 mM | 24 h, 37 °C | 7.9 |
| | 10 mM | 4 h, 37 °C | 4.6 |
| Cysteine | 2 mM | 4 h, RT | <LOD[b] |
| Dimethyl trisulfide | 100 $\mu$M | 4 h, RT | <LOD |
| Lipoic acid | 100 $\mu$M | 4 h, RT | <LOD |
| Dihydrolipoic acid | 100 $\mu$M | 4 h, RT | <LOD |
| $Na_2S_2O_3$ | 100 $\mu$M | 4 h, RT | <LOD |
| $Na_2S_2O_4$ | 100 $\mu$M | 4 h, RT | <LOD |
| NADH | 5 mM | 4 h, RT | <LOD |
| NADPH | 5 mM | 4 h, RT | <LOD |
| NaSCN | 100 $\mu$M | 4 h, RT | <LOD |
| $NaNO_2$ | 100 $\mu$M | 4 h, RT | <LOD |
| NO | 50 $\mu$M | 4 h, RT | <LOD |
| $ONOO^-$ | 100 $\mu$M | 4 h, RT | 1.25 |
| $H_2O_2$ | 100 $\mu$M | 4 h, RT | <LOD |
| *t*-BuOOH | 100 $\mu$M | 4 h, RT | <LOD |
| $O_2^-$ | 1.79 nmol of cytochrome *c*/min | 4 h, RT | <LOD |
| HOCl | 100 $\mu$M | 4 h, RT | <LOD |

[a] RT, room temperature.
[b] LOD, limit of detection.

which rapidly generates $H_2S$ ($pK_a$ = 6.8 (51)), led to the gradual conversion of MitoA to MitoN. RP-HPLC analysis of MitoA following overnight incubation with excess NaHS showed its complete conversion to MitoN (Fig. 2*B*). We could readily detect MitoA and MitoN by mass spectrometry (MS) and their spectra matched those predicted from the natural isotope distribution (supplemental Fig. S2). There was decomposition of MitoA ($[C_{28}H_{26}N_4OP]^+$; predicted *m*/*z* 465.18) by neutral loss of $N_2$ to form the nitrene ($[C_{28}H_{26}N_2OP]^+$; predicted *m*/*z* 437.17), the extent of which depended on MS conditions (Fig. 2*C*). MS analysis of MitoA after overnight incubation with excess NaHS showed formation of MitoN ($[C_{28}H_{29}N_2OP]^+$; predicted *m*/*z* 439.19) further confirming that MitoA reacts with $H_2S$ to form only MitoN (Fig. 2*C*); under these MS conditions only the nitrene product of MitoA was found. When the reaction of MitoA with $H_2S$ was monitored continuously using time-resolved MS, where both MitoA and its nitrene product were observed, the gradual loss of MitoA and the accumulation of MitoN were seen over time, consistent with MitoA reacting selectively with $H_2S$ to generate MitoN (Fig. 2*D*).

The interaction of MitoA with other potential reactive species that it may encounter *in vivo* was assessed by RP-HPLC (Table 1). None of the tested compounds reacted to any significant extent with MitoA to form MitoN (Table 1): the greatest conversion of MitoA to MitoN was 7.9% and required incubation with 10 mM glutathione for 24 h. A significant potential confounder for the selectivity of MitoA for $H_2S$ is the possibility of its reacting with low molecular weight and protein persulfides. Therefore we next assessed the direct reactivity of MitoA with NAP-SSH, a low molecular weight persulfide derivative of *N*-acetylpenicillamine (NAP) (24, 52). A complication of analyzing persulfides is that they spontaneously release $H_2S$, making it difficult to separate the reaction of MitoA with $H_2S$ from that with the persulfide itself (24). To address this, we compared the reaction of MitoA with NAP-SSH to that of MitoA with the same concentration of $H_2S$ (supplemental Fig. S3). These experiments showed the expected reaction of MitoA with $H_2S$ with formation of MitoN, whereas under the same conditions the reaction of MitoA with NAP-SSH to form MitoN was negligible (supplemental Fig. S3). Furthermore, the incubation of 5 $\mu$M persulfidated human serum albumin with 10 $\mu$M MitoA led to negligible (<7%) consumption of MitoA over 4 h at room temperature (data not shown), most probably due to spontaneous decay of persulfides to release $H_2S$ (53).

We next measured the rate of reaction of MitoA with $H_2S$ from the time-dependent disappearance of the MitoA peak at ~270 nm and the appearance of a new peak at 306 nm due to MitoN (Fig. 3*A*). The absorption maxima for the non-TPP aromatic rings were identified using 4-azido-*N*-(hex-1-yl)benzamide and 4-amino-*N*-(hex-1-yl)benzamide, which are analogues of MitoA and MitoN, respectively, but without the TPP targeting group. We then incubated MitoA with known concentrations of $H_2S$ and measured the formation of MitoN at 306 nm (Fig. 3*B*). From these we were able to plot the observed initial rate constant ($k_{obs}$) for MitoN formation against the concentration of $H_2S$ and calculate a rate constant: 0.16 ± 0.03 $M^{-1}$ $s^{-1}$ at 22 °C (Fig. 3*C*). This compares with literature rates for the reaction of $H_2S$ with phenyl azides: 0.12 $M^{-1}$ $s^{-1}$ at 10 °C and 0.95 $M^{-1}$ $s^{-1}$ at 25 °C (37). One concern about the use of MitoA is that its reaction consumes $H_2S$ and generates $H_2S_2$ (37), thereby potentially disrupting $H_2S$ signaling pathways and altering protein persulfidation. Hence the slow reaction of MitoA with $H_2S$ is advantageous because it allows selective detection, while also minimizing disruption to endogenous $H_2S$ signaling pathways. Together these data indicate that, in agreement with other aryl azides (45, 46), MitoA reacts selectively with $H_2S$ and therefore that the conversion of MitoA to MitoN can be used to assess $H_2S$ *in vivo*.

### *Analysis of MitoA and MitoN by LC-MS/MS*

To be useful as an *in vivo* mass spectrometric probe MitoA and MitoN have to be extracted from tissues and analyzed by LC-MS/MS, relative to deuterated internal standards (IS) (47–49). To establish the LC-MS/MS assay we first determined fragmentation conditions that enabled sensitive detection of MitoA and MitoN, and their deuterated internal standards (Fig. 4*A*). For the analysis of MitoA we took into account the neutral loss of $N_2$ from MitoA to generate the nitrene, which under these conditions was complete upon entrance to the first mass spectrometer quadrupole. Using the transitions shown in Fig. 4*A* we could detect MitoA and MitoN, and their deuterated IS, selectively by LC-MS/MS (Fig. 4*B*). Hence we were able to generate standard curves for MitoA and MitoN down to picomole levels (Fig. 4*C*).

A potential concern for the LC-MS/MS analysis is that MitoA might react with $H_2S$ generated upon homogenization and extraction of tissues, for example, by release of labile sulfur from iron-sulfur centers. The possibility of $H_2S$ release was minimized by omitting acid during tissue extraction. Even so, to

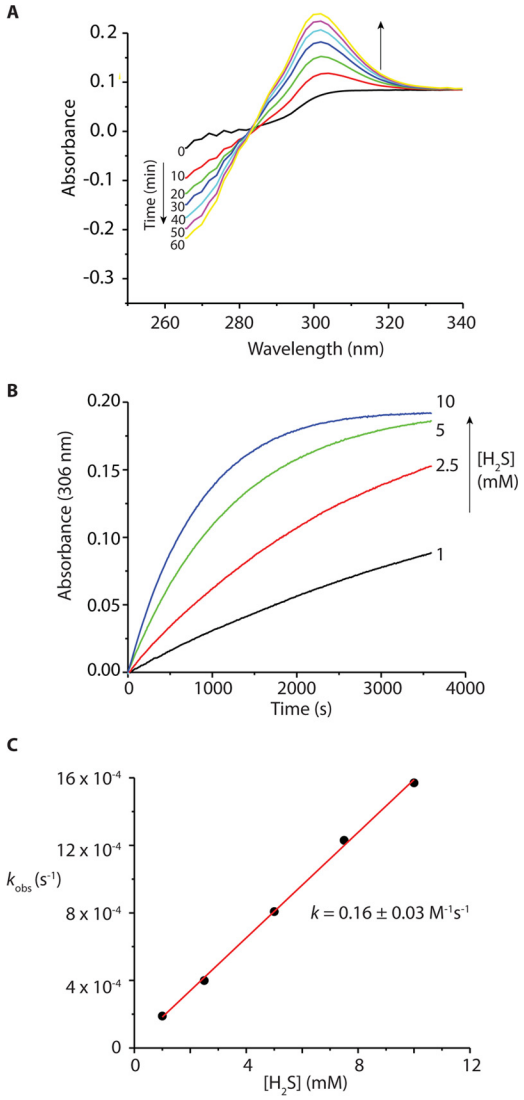


**Figure 3. Rate of reaction of MitoA with $H_2S$ to form MitoN.** *A,* differential time-resolved spectra where 40 $\mu$M MitoA was mixed with 2.5 mM $H_2S$, with MitoA serving as the blank. The spectra illustrate the time-dependent disappearance of the MitoA peak at ~270 nm and the appearance of a new peak assigned to MitoN at ~306 nm. *B,* kinetic traces at 306 nm obtained for the reaction of 40 $\mu$M MitoA with increasing concentrations of $H_2S$, the absorbance was observed over 6 min at 306 nm using a Hewlett Packard 8452A Diode Array Spectrophotometer under pseudo-first order conditions. *C,* plot of $k_{obs}$ *versus* [$H_2S$]. The experiments were performed in 300 mM potassium phosphate buffer, pH 7.4, at 22 °C in triplicates.

assess whether an artifactual reaction with released $H_2S$ could occur, we incubated MitoA in tissue extraction medium supplemented with $H_2S$ for up to 4 h, and then measured MitoN formation by LC-MS/MS. As expected, this showed some conversion of MitoA to MitoN, but with a very small (~0.02) increase in the MitoN/MitoA ratio (supplemental Fig. S4). Considering the high $H_2S$ concentration added, and that the incubation time of 4 h was far longer than that used during conventional extraction, we conclude that the artifactual conversion of MitoA to MitoN during tissue extraction is negligible. In any case such a potential artifact would be equal for all tissue samples and therefore would not affect comparisons. To conclude, we have established a sensitive LC-MS/MS assay for $H_2S$ that can be applied to tissues.

### *Uptake of MitoA and MitoN by mitochondria and cells*

To be useful for the analysis of $H_2S$ *in vivo*, MitoA must be taken up into mitochondria in response to the membrane potential. To see if this occurred we next assessed the accumulation of MitoA and MitoN by isolated mitochondria using a triphenylphosphonium (TPP)-selective electrode (54) (Fig. 5, *A* and *B*). Both probes accumulated inside mitochondria ~650- to ~1,000-fold in response to the membrane potential and this uptake was reversed by abolishing the mitochondrial membrane potential with the uncoupler FCCP. Therefore, MitoN and MitoA are taken up by energized mitochondria as expected for TPP compounds. To determine whether MitoA was accumulated within cells we first established that the toxicity of MitoA or MitoN to cells *in vitro* was negligible at concentrations up to 12.5 $\mu$M, determined by following the effects of the compounds on cell proliferation (supplemental Fig. S5). To assess the uptake of MitoA into cells, we incubated HCT116 cells with MitoA and measured the amounts taken up by the cells over time by LC-MS/MS (Fig. 5*C*). This showed that MitoA was taken up into cells over time, coming to a steady state after ~1 h. Over this time the amount of MitoN generated was small (Fig. 5*C*), consequently the MitoN/MitoA ratio stayed low and constant throughout the incubation (Fig. 5*D*). Therefore MitoA is taken up by cells and, at least under these conditions, there was low MitoN formation.

### *Reactivity and stability of MitoA in tissue homogenates*

MitoA is designed to assess $H_2S$ in tissues *in vivo*. To determine whether there were any enzymatic processes in tissues that could convert MitoA to MitoN in the absence of $H_2S$, we incubated MitoA with liver homogenates and measured MitoN formation (Fig. 6*A*). Under these conditions enzymes are available to react with MitoA, but the lack of tissue and cell architecture means that any $H_2S$ generated will diffuse away. Incubation of MitoA with a liver homogenate led to a negligible MitoN formation (Fig. 6*A*) and no increase in the MitoN/MitoA ratio (Fig. 6*B*), even though the reaction proceeded readily when $H_2S$ was added (Fig. 6, *A* and *B*). Similarly, incubation of MitoN with a liver homogenate in the presence or absence of $H_2S$ led to very little loss of the compound (Fig. 6*C*). Together these data suggest that MitoA conversion to MitoN in tissues is negligible in the absence of $H_2S$, and that once formed MitoN is stable.

### *Response of MitoA to $H_2S$ in ischemic liver sections*

The next step was to see how MitoA responded to an increase in endogenous $H_2S$ within a tissue. To assess this we incubated liver tissue sections with various concentrations of MitoA at 4 °C, designed to mimic conditions during organ storage for transplantation (55, 56). MitoA was taken up into the tissue sections over time (Fig. 6*D*). Under these conditions the tissue will be largely ischemic, as there is no perfusion and $O_2$ will be depleted by the oxidation of endogenous substrates. The lack of $O_2$ will block the activity of the mitochondrial SQR, which is the major way in which $H_2S$ is degraded *in vivo* (Fig. 1*A*). It is known that when the activity of the SQR is decreased by depletion of the mitochondrial CoQ pool, that there is an accumulation of $H_2S$ within mice *in vivo* (57). Thus, under ischemic conditions

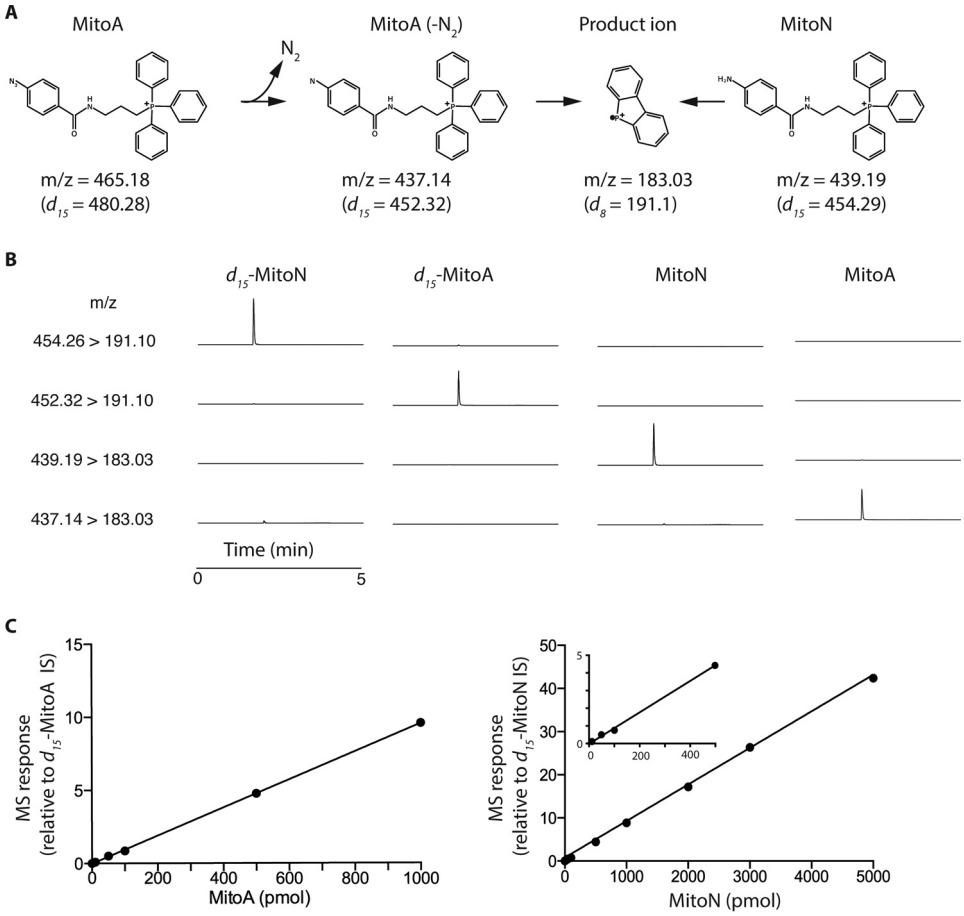


**Figure 4. Detection of MitoA and MitoN by LC-MS/MS.** *A,* the transitions used for analysis of MitoA and MitoN, and their deuterated derivatives, are shown. *B,* typical chromatograms showing the *m/z* transitions measured simultaneously for 50 pmol of $d_{15}$-MitoA, MitoA, $d_{15}$-MitoN, or MitoN. Each trace is normalized to the highest total ion count peak within that trace. *C,* typical standard curves for MitoA and MitoN detection by LC-MS/MS. Samples were prepared in 20% ACN, 0.1% FA and contained known MitoA or MitoN concentrations and their deuterated internal standards. Each point is mean ± range of duplicate measurements.

the inhibition of SQR is expected to increase $H_2S$ levels. Furthermore, $H_2S$ production by the mitochondrial 3-mercaptopyruvate sulfurtransferase enzyme is driven by the reduced form of thioredoxin, which will also increase in concentration upon ischemia (58). Therefore it is likely that there will be an increase in $H_2S$ levels in these liver sections upon ischemia.

To see if this increase in $H_2S$ led to MitoN formation in the ischemic liver sections, we measured MitoN levels over time and expressed these relative to MitoA. This showed an increase in the MitoN/MitoA ratio over time (Fig. 6*E*), consistent with increased $H_2S$ formation in ischemic organs over time. Importantly, the MitoN/MitoA ratios at a given time point were similar for all initial MitoA concentrations used. Thus the ratiometric analysis of MitoN relative to MitoA corrects for differences in MitoA content and suggests that the MitoA/MitoN ratio is a robust measure of changes in $H_2S$ levels.

### *Uptake and metabolism of MitoA and MitoN within tissues in vivo*

Previously developed exomarkers such as MitoB were administered to mice as a single intravenous (i.v.) bolus injection (47). This approach enabled the compounds to be very rapidly accumulated within tissues *in vivo*, after which they are gradually lost over the following hours. This protocol gives sufficient time for the accumulated compound (*e.g.* MitoB) to react with its target (*e.g.* $H_2O_2$) to form an exomarker (*e.g.* MitoP). To see if MitoA could also be used in this way, we assessed MitoA distribution within mouse tissues following a single i.v. injection (Fig. 7, *A* and *B*). This showed rapid clearance of MitoA from the blood and its accumulation into the heart and liver, but not the brain, as expected for TPP compounds in mice (59, 60) (Fig. 7*A*). The kidney accumulated more MitoA than the other tissues, presumably due to direct removal of the initial bolus from the circulation, as well as redistribution of MitoA from other tissues over time (Fig. 7*B*). MitoA was gradually lost from the tissues over time (Fig. 7, *A* and *B*), consistent with other TPP compounds (59). These findings suggest that MitoA is accumulated rapidly by tissues and is retained long enough to respond to local levels of $H_2S$.

To report on $H_2S$ levels within tissues *in vivo* MitoA should only be converted to MitoN by reaction with $H_2S$, with minimal side reactions. To assess this we injected MitoA into mice and 1 h later isolated the liver. The liver was chosen because it readily accumulates MitoA (Fig. 7*A*) and has extensive xenobiotic metabolism. Thus, if MitoA is biotransformed to compounds other than MitoN *in vivo* the liver should demonstrate this biotransformation. Extraction and MS analysis of the liver showed

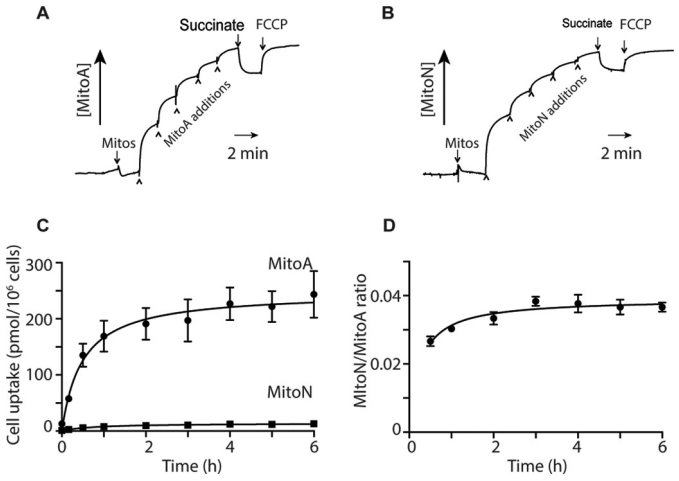


**Figure 5. Accumulation of MitoA and MitoN by isolated mitochondria and cells.** The uptake of MitoA (*A*) and MitoN (*B*) was examined in isolated mitochondria (2 mg of protein/ml) incubated in KCl medium supplemented with 4 $\mu$g/ml of rotenone and 100 nM nigericin using a TPP-selective electrode. The compounds were added in 1 $\mu$M steps, followed by 10 mM succinate and 500 nM FCCP. *C,* MitoA uptake by HCT116 cells. HCT116 cells were plated at 250,000 cells/well (~27,000 cells/cm$^2$) in 6-well plates overnight and then incubated with 10 $\mu$M MitoA in DMEM containing 10% FBS and antibiotics. At various times 1 ml of supernatant was removed for analysis, the rest was discarded, and the cells were rinsed with 1 ml of PBS and collected by scraping into 0.5 ml of PBS and pelleted by centrifugation (16,000 $\times$ *g*, 3 min, room temperature). Cell pellets were snap frozen and stored at −20 °C. Compounds were extracted and quantified by LC-MS/MS. Results are mean ± S.E. for $n = 3$. MitoA levels in the supernatant did not change over 6 h (data not shown). *D,* for the experiment in *C*, the level of MitoN in the cell pellets were assessed in parallel with MitoA and the MitoN/MitoA ratio is shown.

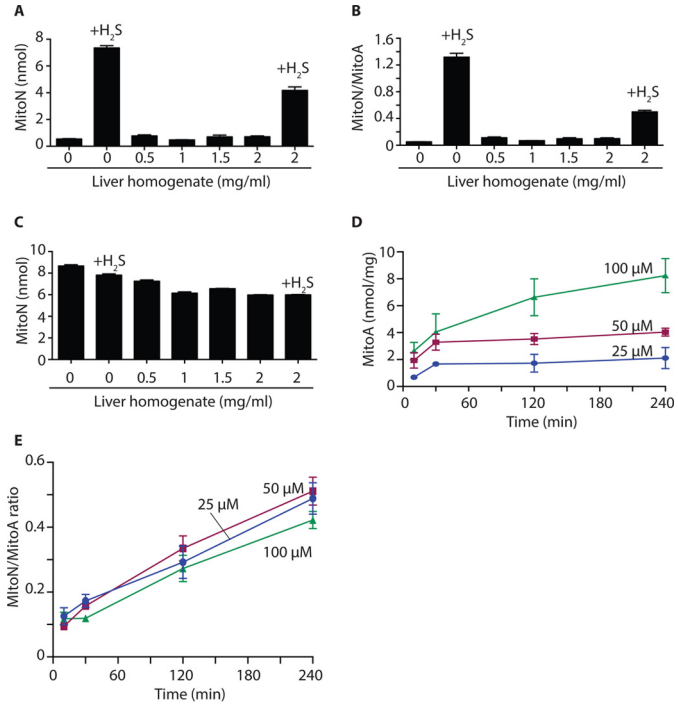


**Figure 6. MitoA and MitoN metabolism in the liver *ex vivo*.** *A* and *B,* MitoA metabolism by a liver homogenate. MitoA (10 $\mu$M) was incubated with various amounts of liver homogenate, or with liver homogenate and NaHS (25 $\mu$M), for 2 h at 37 °C. Samples were then analyzed by LC-MS/MS to quantify MitoA (data not shown), MitoN (*A*), and the MitoN/MitoA ratio (*B*). Data are mean ± S.E., $n = 3$. *C,* MitoN metabolism by a liver homogenate. MitoN (10 $\mu$M) was incubated with various amounts of liver homogenate, or with liver homogenate and NaHS (25 $\mu$M), for 2 h at 37 °C. Samples were then analyzed by LC-MS/MS for MitoN. Data are mean ± S.E., $n = 3$. *D,* uptake of MitoA by liver sections. Rat liver sections of ~20 to 50 mg wet weight were incubated with MitoA in University of Wisconsin solution at 4 °C. After incubation, the tissue pieces were rinsed in PBS, dried, and snap frozen prior to quantification of MitoA and MitoN by LC-MS/MS. Data show the accumulation of MitoA over time and are mean ± S.E., $n = 3$. *E,* MitoN/MitoA ratio in liver sections. The MitoN/MitoA ratio was determined over time in liver sections as described in *D*.

a large number of compounds (Fig. 7*C, i*). Analysis by MS/MS at the transition diagnostic for MitoA (437 > 183) showed the presence of MitoA (Fig. 7*C, ii*). Similarly, analysis at the transition diagnostic for MitoN (439 > 183) showed some MitoN formation *in vivo* (Fig. 7*C, iii*). These mass spectra were identical to those of pure MitoA and MitoN (Fig. 7*C, ii* and *iii*, *insets*). To see if MitoA and MitoN were metabolized in the liver to other TPP containing molecules, we next carried out a precursor scan of the extract to identify all compounds that fragmented to a product with *m*/*z* 183, diagnostic of a TPP-containing compound (47, 61). In the liver extract the only precursor molecules that gave a product ion of *m*/*z* 183 corresponded to the nitrene product of MitoA upon neutral loss of $N_2$ (*m*/*z* 437), MitoN (*m*/*z* 439), with a small amount of intact MitoA (*m*/*z* 465) (Fig. 7*C, iv*). This precursor ion pattern was similar to that of pure MitoA (Fig. 7*C, iv*, *inset*).

Another potential concern is whether MitoN could be further metabolized *in vivo*, following its formation from MitoA. To assess this we injected MitoN into mice and 1 h later isolated the liver and analyzed this extract by MS analysis (Fig. 7*D, i*). Analysis by MS/MS at the transition diagnostic for MitoN (439 > 183) showed the presence of MitoN (Fig. 7*D, ii*), and the spectrum was identical to that of pure MitoN (Fig. 7*D, ii, inset*). To see if MitoN was metabolized within the liver *in vivo*, we next carried out a precursor scan of the extract to identify all compounds that fragmented to a product with *m*/*z* 183, diagnostic of a TPP containing compound (47, 61). In the liver homogenate the only parent molecules that gave a daughter ion of *m*/*z* 183 corresponded to MitoN (*m*/*z* 439), with a small peak at 455 (Fig. 7*D, iii*). This precursor ion pattern was similar to that of pure MitoN (Fig. 7*D, iii*, *inset*). The precursor ion at 455 is a +16 shift from MitoN and may represent oxidation of MitoN by addition of an oxygen atom. Even so, it suggests that once formed MitoN is relatively stable and that any further metabolism of MitoN is unlikely to affect the analysis of $H_2S$ *in vivo*.

### *Use of MitoA to analyze $H_2S$ in the ischemic heart in vivo*

The increase in the MitoN/MitoA ratio in the ischemic liver (Fig. 6*E*) is consistent with an increase in $H_2S$ in tissue during ischemia. To extend this, we next focused on the heart as its metabolism changes dramatically upon ischemia (62, 63). As a first step to see whether there was any accumulation of $H_2S$ in the ischemic heart we administered MitoA to mice, isolated the heart, and stored it under ischemic conditions mimicking those used for organ storage during transplantation (Fig. 8*A*). The MitoN/MitoA ratio increased after 240 min ischemia, consistent with elevated $H_2S$ during the ischemia inherent in organ storage.

To explore further how $H_2S$ levels respond to ischemia we next used the left anterior descending (LAD) model of acute myocardial infarction. MitoA was injected into mice and then

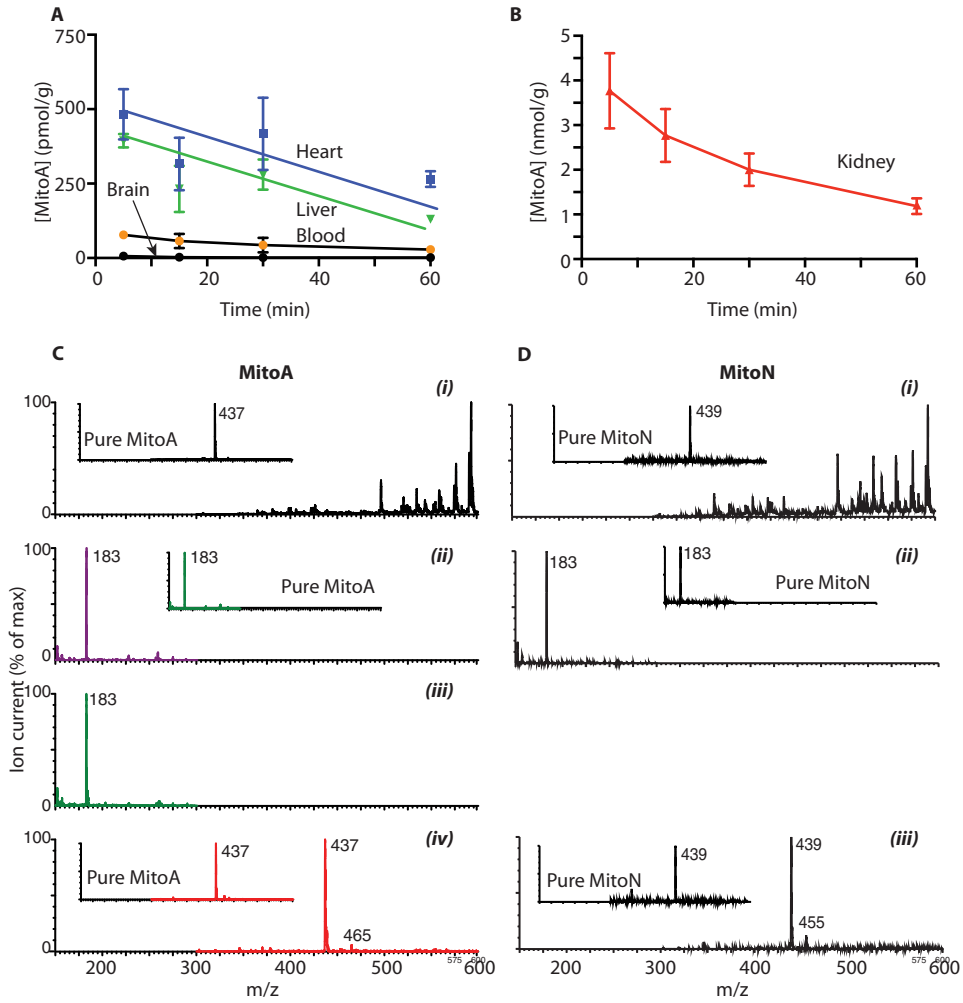


**Figure 7. Uptake and metabolism of MitoA *in vivo*.** *A* and *B,* mice were injected with 50 nmol of MitoA and tissues were collected, extracted, and analyzed by LC-MS/MS. Results are mean ± S.E., $n = 3$. *C*, MitoA (50 nmol) was administered to mice. After 60 min the liver was collected, extracted, and prepared as for mass spectrometry (LC-MS/MS) but omitting the internal standards and analyzed by mass spectrometry by direct infusion at 5 $\mu$l/min. *C, i,* shows the mass spectrum of the liver extract. *ii,* shows the MS/MS spectrum of the liver extract assessed for MitoA (437 > 183). The *inset* shows the MS/MS spectrum for pure MitoA. *iii,* shows the MS/MS spectrum of the liver extract assessed for MitoN (439 > 183). The *inset* shows the MS/MS spectrum for pure MitoN. *iv,* shows the precursor scan of the liver extract assessed for precursor ions that generate a product ion of *m/z* 183. The *inset* shows the precursor ion scan for pure MitoA. *D,* MitoN (50 nmol) was administered to mice. After 60 min the liver was collected, extracted into solvent, and prepared as for mass spectrometry, but omitting the internal standards, and analyzed by MS by direct infusion at 5 $\mu$l/min. *D*, *i*, shows the mass spectrum of the liver extract. *ii*, shows the MS/MS spectrum of the liver extract assessed for MitoN (439 > 183). The *inset* shows the MS/MS spectrum for pure MitoN. *iii*, shows the precursor scan of the liver extract assessed for precursor ions that generate a product ion of *m/z* 183. The *inset* shows the precursor ion scan for pure MitoN. For all spectra the maximum ion counts are indicated on the spectra and all ion counts are expressed as % of the maximum.

cardiac ischemia was induced by closing off the LAD artery, thus subjecting a large section of the left ventricle to ischemia. In previous work we have shown that when the occlusion to the LAD artery was removed after 30 min ischemia and the tissue reperfused with oxygenated blood, there was extensive ischemia-reperfusion injury (63). This model thereby enables us to use MitoA to assess variations of $H_2S$ levels during both ischemia and reperfusion. In comparing the formation of MitoN through these changes it is important that MitoA is present in the tissue for the same duration. To ensure this, we injected MitoA at various time points before or after initiation of ischemia (Fig. 8*B*). Importantly, this protocol meant that MitoA was exposed to a range of times of ischemia and reperfusion, whereas always being present in the tissue for 40 min, thereby facilitating comparison. In the LAD model only the left ventricle is exposed to ischemia and reperfusion, however, as it was unclear what effect ischemia in the left ventricle would have on the right ventricle from the same mouse, the right ventricle from the same mouse cannot act as a control. Therefore the left and right ventricles from mice that underwent ischemia were compared with the appropriate ventricle from MitoA-treated normoxic mice.

When MitoA was injected into control mice in which the hearts were not exposed to ischemia or reperfusion, analysis of the right and left ventricles 40 min later showed a low MitoN/MitoA ratio in both ventricles (Fig. 8*C*). When MitoA was injected before reperfusion, the MitoN/MitoA ratio was increased compared with normoxic hearts, presumably as result of $H_2S$ present in the tissue before reperfusion. However, administration 5 min after reperfusion resulted in the MitoN/MitoA ratio similar to normoxic hearts. Furthermore, during ischemia there was a dramatic increase in the MitoN/MitoA

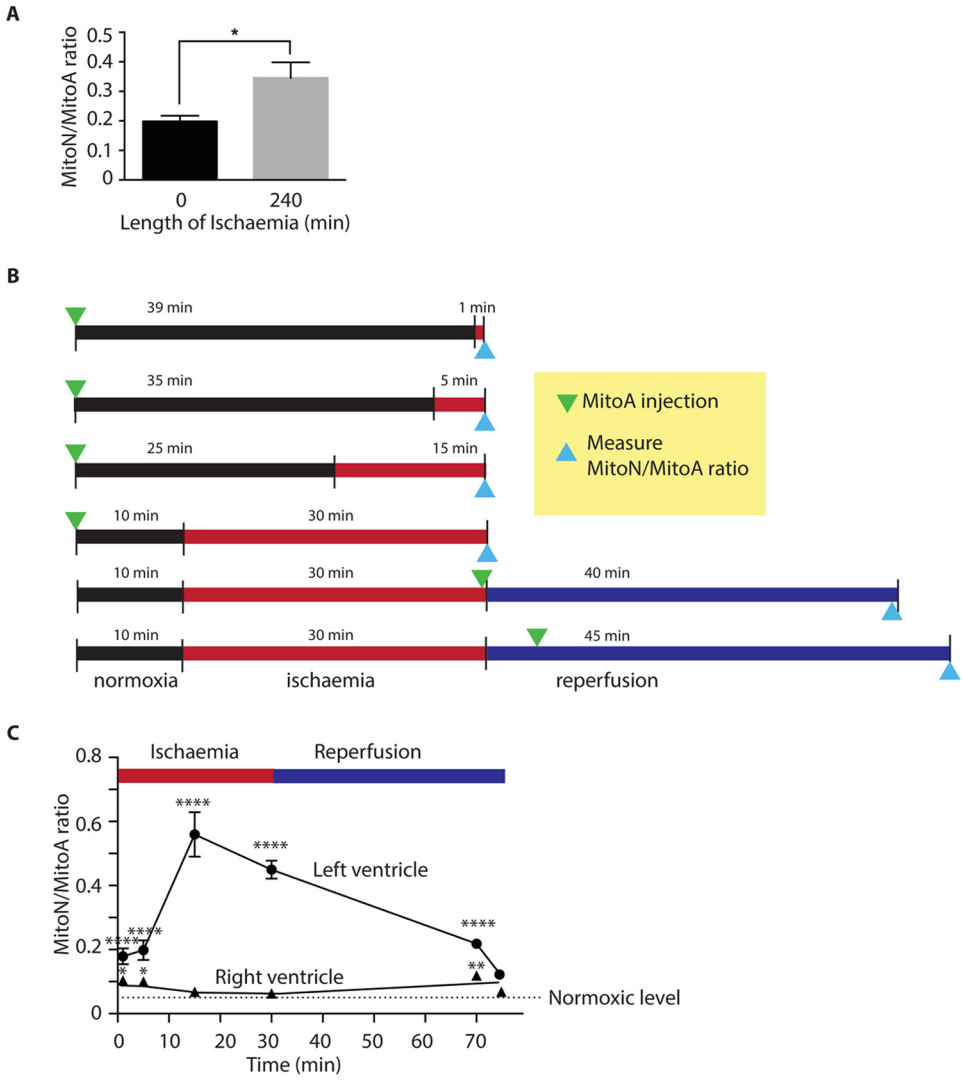


**Figure 8. Assessment of $H_2S$ *in vivo* using MitoA.** *A,* MitoA in the heart during storage *ex vivo*. MitoA (50 nmol) was administered to mice via tail vein injection. The heart was removed after ~12 min of warm ischemia. The hearts were then either snap frozen or stored for 240 min on ice and then snap frozen. Samples were analyzed by LC-MS/MS for MitoA and MitoN, and the MitoN/MitoA ratio was calculated. Results are mean ± S.E., $n = 3$. *, $p < 0.05$ by Student's two-tailed *t* test. *B,* protocol for the LAD artery occlusion experiments. *C,* mice were injected with 50 nmol of MitoA prior to ischemia of the left ventricle induced by occlusion of the LAD artery. At the end of the protocol the hearts were separated into right (normoxic) and left (normoxic or ischemic) ventricles, snap frozen, and analyzed for MitoA and MitoN content by LC-MS/MS, enabling the MitoN/MitoA ratio to be calculated. Data are mean ± S.E., $n = 3$. *, $p < 0.05$; **, $p < 0.01$; ***, $p < 0.001$; ****, $p < 0.0001$, by two-way analysis of variance followed by post hoc Bonferroni test.

ratio in the left ventricle, but not in the right (Fig. 8*C*). The MitoN/MitoA ratio increased the longer the duration of ischemia to which the left ventricle was exposed (Fig. 8*C*). Comparison between the ischemic and non-ischemic zones of the heart showed that the $H_2S$ increase was local to the ischemic tissue area, and did not diffuse to surrounding tissue of the same organ. Together, these findings are consistent with an increase in $H_2S$ during ischemia that is rapidly reversed once oxygen is reintroduced into the tissue upon reperfusion. Furthermore, these findings indicate that MitoA can be used to assess changes in $H_2S$ *in vivo*.

## Conclusions

Here we have applied the exomarker approach to the analysis of $H_2S$ *in vivo*. To do this we used the well established chemistry of aryl azides and their conversion to an amine on reaction with $H_2S$ (33, 36, 46). The combination of this chemistry with mitochondria targeting by the TPP moiety led to its rapid uptake into cells *in vivo* where it is predicted to be mainly located in the mitochondria. There, MitoA should react with $H_2S$ to form the diagnostic exomarker MitoN. The chemical selectivity for $H_2S$ of the MitoA probe was clear, and it did not react with other potential factors found in biological environments. Most importantly, it did not react directly with persulfides, suggesting that *in vivo* it reports on free $H_2S$ independently of any changes in the levels of protein or low molecular weight persulfides.

The most important aspect of the development of MitoA is that it enables the assessment of changes in $H_2S$ *in vivo*. This exomarker approach has previously been used to infer levels of evanescent species such as $H_2O_2$ in a range of living organisms, where assessments *ex vivo* or in isolated cells would have introduced confounding factors making the data hard to interpret. The experimental constraints are similar with assessment of

free $H_2S$ in tissues, and are in fact exacerbated due to the rapid diffusion of $H_2S$ from *in vitro* systems, such as cell culture where $H_2S$ rapidly disperses into the large amount of medium above a cell monolayer and is then lost into the head space. In contrast, in tissues the situation is quite different, where the local architecture can enable a large build up of $H_2S$. Consequently, measurements of $H_2S$ levels within tissues *in vivo* under normal and pathological conditions are essential to infer the roles of $H_2S$ *in vivo*.

As a proof of principle to test MitoA *in vivo*, we assessed changes in $H_2S$ in tissues undergoing ischemia/hypoxia. Ischemia is expected to lead to an increase in $H_2S$ due to the inhibition of $H_2S$ degradation by SQR that occurs in the absence of $O_2$. An advantage of this model to test the efficacy of MitoA was that there was no intervention with an exogenous agent or $H_2S$ donor, thus it indicates that MitoA can respond to $H_2S$ levels that may arise *in vivo* under pathological conditions. These findings also demonstrated that there were dramatic changes in $H_2S$ between the ischemic and normoxic regions of the heart, and that the $H_2S$ levels rapidly returned to normal upon reperfusion with oxygenated blood. None of these assessments would have been possible prior to the development of MitoA. Interestingly, as well as enabling the testing of MitoA, these findings suggested that $H_2S$ levels may be a significant aspect of how tissues respond to ischemia and these changes in $H_2S$ will be explored further as a potential ischemic signaling pathway.

There are a few limitations to the exomarker approach. Because the ratio of MitoN to MitoA can only be determined from tissue samples *ex vivo*, each time point requires killing a mouse. Furthermore, the analysis is inevitably an average of many different cells and mitochondria. Consequently, complementary techniques are required to assess changes in individual cells and in real time. Another caveat is that many of the effects of altering $H_2S$ metabolism are likely to be caused by changes in protein persulfidation that will not be picked up directly by the MitoA approach, which only responds to free $H_2S$. Therefore it is important in the future to develop related techniques to assess protein persulfidation in parallel to the measurement of free $H_2S$. Finally, it is difficult to relate the MitoN/MitoA ratio to the actual amount of $H_2S$ present *in vivo*.

In summary, we have developed a mass spectrometric probe that will enable for the first time changes in the levels of $H_2S$ to be assessed *in vivo*. Use of this probe will greatly facilitate investigations of the role of $H_2S$ in health and disease.

## Experimental procedures

### Chemical syntheses

MitoA and MitoN were synthesized from triphenylphosphine and the deuterated analogues, $d_{15}$-MitoA and $d_{15}$-MitoN, from tri(pentadeuterophenyl)phosphine as shown in supplemental Fig. S1A. The triarylphosphines were each reacted with 1,3-diodopropane to give iodopropyl-TPP salts **1** and $\boldsymbol{d_{15}}$**-1**. Displacement of the alkyl iodide by azide gave the azidopropyl-TPP salts **2** and $\boldsymbol{d_{15}}$**-2**, and hydrogenation converted these into the amines **3** and $\boldsymbol{d_{15}}$**-3**. The latter were coupled with 4-azidobenzoic acid using diisopropylcarbodiimide in acetonitrile (ACN) and the resulting amide precipitated from solution in each case. Ion exchange then gave MitoA and $d_{15}$-MitoA as their mesylate salts in moderate yield. In a similar way, coupling 4-aminobenzoic acid followed by ion exchange gave MitoN and $d_{15}$-MitoN as their mesylate salts. 4-Azido-*N*-(hex-1-yl)benzamide **4** and 4-amino-*N*-(hex-1-yl)benzamide **5**, which are analogues of MitoA and MitoN lacking the TPP targeting group, were prepared for comparison (supplemental Fig. S1B). Further details of the chemical syntheses are given under supplementary materials. Peroxynitrite was prepared according to Refs. 64 and 65. A persulfide analogue of *S*-nitrosopenicillamine, NAP-SSH, was synthesized as described (52) and was prepared as a 1 mM stock in 10 mM HCl at 4 °C.

### Assessment of compound properties

MitoA and MitoN stock solutions (5 mM in ethanol (EtOH)) were stable for at least 6 months at −20 °C. Absorbance spectra were carried out in 1-ml cuvettes in KCl buffer (120 mM KCl, 10 mM Hepes and 1 mM EGTA, pH 7.2 (KOH)) using a Shimadzu UV-2501PC UV-visible spectrophotometer. The molar extinction coefficient for MitoA at 267 nm in KCl buffer was calculated gravimetrically: $20.4 \pm 0.1 \times 10^3\ \text{M}^{-1}\ \text{cm}^{-1}$.

Reversed phase-high performance liquid chromatography (RP-HPLC) was done using a Gilson 321 pump with attached UV-visible 151 system (Gilson). Samples were filtered through a 0.22-$\mu$m polyvinylidene difluoride (PVDF) filter (Millex, Millipore), loaded, and run over a $C_{18}$ column (Jupiter 300 Å, Phenomenex) with a Widepore $C_{18}$ guard column (Phenomenex). HPLC buffer A (0.1% (v/v) trifluoroacetic acid (TFA) in water) and HPLC buffer B (0.1% (v/v) TFA/acetonitrile) were used with the gradient: 0–2 min, 5% B; 2–17 min, 5–100% B; 17–19 min, 100% B; 19–22 min 100–5% B.

### Cell culture

Cells (C2C12 or HCT116 from the American Type Culture Collection) were incubated at 37 °C in a humidified atmosphere of 95% air and 5% $CO_2$ in Dulbecco's modified Eagle's medium (Invitrogen) supplemented with 10% (v/v) fetal bovine serum (FBS) and 100 units/ml of penicillin and 100 $\mu$g/ml of streptomycin.

### Preparation of $H_2S$ solutions

Unless indicated otherwise, standard solutions of $H_2S$ were prepared by dissolving NaHS in KCl buffer, the pH was re-adjusted to 7.2 and then the solution was aliquoted into tubes with no head space and kept on ice. The $H_2S$ concentration was determined by the methylene blue assay (66).

### Mitochondrial preparation and incubation

Liver mitochondria were prepared from female Wistar rats killed by stunning and cervical dislocation, followed by homogenization of the liver and differential centrifugation in ice-cold STE buffer (250 mM sucrose, 10 mM Tris, 1 mM EGTA, pH 7.4). The protein concentration was determined by the biuret assay using bovine serum albumin as a standard (67).

### Extraction of MitoA and MitoN

For cells, frozen pellets were thawed, vortexed, and resuspended in 210 $\mu$l of 95% acetonitrile (ACN) spiked with internal

standard (100 pmol of $d_{15}$-MitoA and 100 pmol of $d_{15}$-MitoN). Following protein precipitation (30 min, 4 °C) and centrifugation (16,000 × *g*, 10 min, room temperature) the supernatant was filtered through a 0.22-μm filter and dried under vacuum (miVac Quattro concentrator; Genevac) and stored at −20 °C. For extraction from tissues, ~50 mg wet weight tissue was placed in a 2-ml Eppendorf tube containing 210 μl of 95% ACN spiked with internal standards (100 pmol of $d_{15}$-MitoA and 100 pmol of $d_{15}$-MitoN). For the blood no further additions were made, but for the tissues we added ~50 μl of beads (liver, brain, and kidney, 0.5-mm diameter zirconium oxide beads; heart, 0.9–2.0-mm diameter stainless steel beads, both from Next Advance) and homogenized for 3 min using a Bullet Blender (Storm 24; Next Advance) at speed 8. Samples were centrifuged (16,000 × *g*, 10 min, room temperature), the supernatant was transferred to a new Eppendorf tube. The pellet was re-extracted with 95% ACN, and the supernatants were pooled and incubated for 30 min at 4 °C to precipitate proteins. After centrifugation (16,000 × *g*, 10 min, room temperature) the supernatant was filtered and dried as above and stored at −20 °C. Prior to analysis the samples were resuspended in 20% ACN, 0.1% FA, centrifuged (16,000 × *g*, 10 min, room temperature), and transferred to mass spectrometry vials (TrueView™ LCMS Certified, Waters).

### *LC-MS/MS analysis*

For MS/MS analysis we used a triple-quadrupole mass spectrometer (Waters Xevo TQ-S under positive ion mode: source spray voltage, 3.2 kV; cone voltage, 125 V; ion source temperature, 100 °C; collision energy, 75 V). Nitrogen and argon were used as curtain and collision gas, respectively. MS fragmentation patterns were determined by direct infusion (5 nM at 50 μl/min in 20% ACN, 0.1% FA). For LC-MS/MS analyses the mass spectrometer was connected in series to an I-class Acquity LC system (Waters). Samples were stored in an autosampler at 4 °C and 2-μl samples went into a 15-μl flow-through needle and RP-UPLC at 40 °C using an Acquity UPLC® BEH C18 column (1 × 50 mm, 1.7 μm; Waters) with a Waters UPLC filter (0.2 μm). MS buffers A (95% water, 5% ACN, 0.1% FA) and B (90% ACN, 10% water, 0.1% FA) were infused at 200 μl/min using the following gradient: 0–0.3 min, 5% B; 0.3–3 min, 5–100% B; 3–4 min, 100% B, 4.0–4.10, 100–105% B; 4.10–4.60 min, 5% B. Eluant was diverted to waste from 0 to 1 min and from 4 to 4.6 min. Compounds were detected in multiple reactions monitoring in positive ion mode. Under these conditions MitoA underwent neutral loss of $N_2$ to a nitrene, which was used as the precursor ion. For quantification the following transitions were used: MitoA, 437 > 183; $d_{15}$-MitoA, 452 > 191; MitoN, 439 > 183; $d_{15}$-MitoN, 454 > 191. Standard curves with known amounts of MitoA and MitoN were prepared, spiked with IS, and extracted following the protocol outlined above. The peak area of MitoA, MitoN, and IS of samples and standard curves were quantified using the MassLynx 4.1 software.

### *Liver homogenate incubations*

Liver was collected from a female Wistar rat that had been killed by stunning and cervical dislocation, and carried out in accordance with the UK Home Office Guide on Animal Experiments. The liver was transferred to ice-cold STE buffer, cut into small pieces using a razor blade, washed in ice-cold KCl buffer, and homogenized in a Dounce homgenizer, and the protein concentration was determined by biuret assay.

### *Mouse experiments*

Wild-type male C57BL/6J mice (8–10 weeks old) were obtained from Charles Rivers Laboratories (UK). Mice were housed under standard laboratory conditions with food and water available *ad libitum* and experiments were carried out in accordance with the UK Home Office Guide on Animal Experiments and were approved under Project Licenses PPL 70/8238, 70/7963, and PPL 80/2638. To assess MitoA uptake and distribution *in vivo*, mice were placed in a heating chamber set to 38 °C (Vet-Tech Solutions) for ~5 min, inserted in a rodent restrainer with free access to the tail, and MitoA (50 nmol) was injected into a lateral tail vein in 100 μl of saline through a 27-gauge needle connected to a 1-ml syringe. Mice were then monitored throughout the incubation period until time points for tissue collection were reached.

For the *ex vivo* incubation of hearts, mice were anesthetized with isoflurane (Abbott Laboratories, US) and oxygen at 2 liters/min. MitoA (50 nmol) was administered in saline via the inferior vena cava and then the heart was explanted as described (68). In brief, 100 μl of heparin was administered prior to exsanguination by division of the inferior vena cava and aorta. The inferior vena cava, hemiazygous vein, superior vena cava, innominate, left carotid, and left brachiocephalic were ligated prior to division of the descending aorta, pulmonary artery, and pulmonary veins. The heart was perfused with 500 μl of ice-cold Soltran (Baxter Healthcare, UK). During dissection and ligation of vessels the heart was topically cooled with 4 °C saline every 2 min. This process took 12 min and the heart was excised and stored in 10 ml of Belzer UW® Cold Storage Solution, University of Wisconsin solution (Belzer UW® Cold Storage Solution, Bridge to Life Ltd.) on ice for 240 min or snap frozen immediately. Samples were stored at −80 °C until extraction for LC-MS/MS.

*In vivo* IRI was performed by using an open-chest, *in situ* mouse (C57BL/6J) heart model in which the LAD is surgically transiently occluded as recently described (69). Mice were anesthetized (pentobarbital sodium; 70 mg/kg; intraperitoneal (i.p.)), intubated endotracheally, and ventilated with 3 cm of $H_2O$ positive end-expiratory pressure (110 breaths per min, 125–150 ml tidal volume) using a mouse ventilator (MINIVENT Type 845, Harvard Apparatus, Germany). Body temperature was monitored by rectal probe and maintained at 37 °C via an animal temperature controller (TCAT-2LV, Physitemp, Clifton, NJ). Corneal and withdraw reflexes were checked for anesthesia depth and additional anesthesia was administered throughout the experimental protocol if needed. A left thoracotomy was performed and the heart was exposed via stripping of the pericardium. Regional ischemia was then induced via ligation of the main branch of the LAD. Successful occlusion was confirmed by color change of the anterior wall of the left ventricle and apex from a bright red color typical of a perfused heart to off-white and ischemia was sustained for 30 min, at which point the tissue was reperfused.

Reperfusion of the heart was confirmed by a color change of the ischemic zone to red. Control mice were sham treated. MitoA (50 nmol) was administered as a 100-$\mu$l bolus via the tail vein at various times during the procedure. Tissue was collected, snap frozen, and stored at −80 °C until analysis.

*Author contributions*—S. A. characterized MitoA and MitoN. C. B.-G. synthesized MitoA and MitoN. A. L. and S. A. carried out the mass spectrometric analyses. T. R. carried out the mouse LAD experiments. T. A. P. processed samples for mass spectrometry and carried out the ion-selective electrode experiments, J. M. and K. S.-P. carried out the heart storage in transplantation medium experiments, T. K. supervised the mouse LAD experiments. M. R. F. and R. W. carried out the kinetic studies. R. C. H. supervised the chemical synthesis and helped direct the project and write the manuscript. M. P. M. and R. C. H. directed the project and wrote the manuscript, with assistance from all other authors.

*Acknowledgment—We are grateful to Professor Christopher J. Chang, University of California at Berkeley, for helpful discussions.*

## References


1. Abe, K., and Kimura, H. (1996) The possible role of hydrogen sulfide as an endogenous neuromodulator. *J. Neurosci.* **16,** 1066–1071
2. Wang, X., Wang, Q., Guo, W., and Zhu, Y. Z. (2011) Hydrogen sulfide attenuates cardiac dysfunction in a rat model of heart failure: a mechanism through cardiac mitochondrial protection. *Biosci. Rep.* **31,** 87–98
3. Li, L., Hsu, A., and Moore, P. K. (2009) Actions and interactions of nitric oxide, carbon monoxide and hydrogen sulphide in the cardiovascular system and in inflammation: a tale of three gases! *Pharmacol. Ther.* **123,** 386–400
4. Li, L., Bhatia, M., Zhu, Y. Z., Zhu, Y. C., Ramnath, R. D., Wang, Z. J., Anuar, F. B., Whiteman, M., Salto-Tellez, M., and Moore, P. K. (2005) Hydrogen sulfide is a novel mediator of lipopolysaccharide-induced inflammation in the mouse. *FASEB J.* **19,** 1196–1198
5. Whiteman, M., and Winyard, P. G. (2011) Hydrogen sulfide and inflammation: the good, the bad, the ugly and the promising. *Expert Rev. Clin. Pharmacol.* **4,** 13–32
6. Szabo, C., Ransy, C., Módis, K., Andriamihaja, M., Murghes, B., Coletta, C., Olah, G., Yanagi, K., and Bouillaud, F. (2014) Regulation of mitochondrial bioenergetic function by hydrogen sulfide: part I. biochemical and physiological mechanisms. *Br. J. Pharmacol.* **171,** 2099–2122
7. Kimura, H., Nagai, Y., Umemura, K., and Kimura, Y. (2005) Physiological roles of hydrogen sulfide: synaptic modulation, neuroprotection, and smooth muscle relaxation. *Antioxid. Redox Signal.* **7,** 795–803
8. Yang, G., Wu, L., Jiang, B., Yang, W., Qi, J., Cao, K., Meng, Q., Mustafa, A. K., Mu, W., Zhang, S., Snyder, S. H., and Wang, R. (2008) $H_2S$ as a physiologic vasorelaxant: hypertension in mice with deletion of cystathionine γ-lyase. *Science* **322,** 587–590
9. Calvert, J. W., Coetzee, W. A., and Lefer, D. J. (2010) Novel insights into hydrogen sulfide: mediated cytoprotection. *Antioxid. Redox Signal.* **12,** 1203–1217
10. Calvert, J. W., Jha, S., Gundewar, S., Elrod, J. W., Ramachandran, A., Pattillo, C. B., Kevil, C. G., and Lefer, D. J. (2009) Hydrogen sulfide mediates cardioprotection through Nrf2 signaling. *Circ. Res.* **105,** 365–374
11. Kondo, K., Bhushan, S., King, A. L., Prabhu, S. D., Hamid, T., Koenig, S., Murohara, T., Predmore, B. L., Gojon, G., Sr., Gojon, G., Jr., Wang, R., Karusula, N., Nicholson, C. K., Calvert, J. W., and Lefer, D. J. (2013) $H_2S$ protects against pressure overload-induced heart failure via upregulation of endothelial nitric oxide synthase. *Circulation* **127,** 1116–1127
12. King, A. L., and Lefer, D. J. (2011) Cytoprotective actions of hydrogen sulfide in ischaemia-reperfusion injury. *Exp. Physiol.* **96,** 840–846
13. Johansen, D., Ytrehus, K., and Baxter, G. F. (2006) Exogenous hydrogen sulfide ($H_2S$) protects against regional myocardial ischemia-reperfusion injury: evidence for a role of K ATP channels. *Basic Res. Cardiol.* **101,** 53–60
14. Wen, Y. D., Wang, H., Kho, S. H., Rinkiko, S., Sheng, X., Shen, H. M., and Zhu, Y. Z. (2013) Hydrogen sulfide protects HUVECs against hydrogen peroxide induced mitochondrial dysfunction and oxidative stress. *PloS One* **8,** e53147
15. Elrod, J. W., Calvert, J. W., Morrison, J., Doeller, J. E., Kraus, D. W., Tao, L., Jiao, X., Scalia, R., Kiss, L., Szabo, C., Kimura, H., Chow, C. W., and Lefer, D. J. (2007) Hydrogen sulfide attenuates myocardial ischemia-reperfusion injury by preservation of mitochondrial function. *Proc. Natl. Acad. Sci. U.S.A.* **104,** 15560–15565
16. Kang, J., Li, Z., Organ, C. L., Park, C. M., Yang, C. T., Pacheco, A., Wang, D., Lefer, D. J., and Xian, M. (2016) pH-controlled hydrogen sulfide release for myocardial ischemia-reperfusion injury. *J. Am. Chem. Soc.* **138,** 6336–6339
17. Blackstone, E., Morrison, M., and Roth, M. B. (2005) $H_2S$ induces a suspended animation-like state in mice. *Science* **308,** 518
18. Derwall, M., Francis, R. C., Kida, K., Bougaki, M., Crimi, E., Adrie, C., Zapol, W. M., and Ichinose, F. (2011) Administration of hydrogen sulfide via extracorporeal membrane lung ventilation in sheep with partial cardiopulmonary bypass perfusion: a proof of concept study on metabolic and vasomotor effects. *Crit. Care* **15,** R51
19. Drabek, T., Kochanek, P. M., Stezoski, J., Wu, X., Bayir, H., Morhard, R. C., Stezoski, S. W., and Tisherman, S. A. (2011) Intravenous hydrogen sulfide does not induce hypothermia or improve survival from hemorrhagic shock in pigs. *Shock* **35,** 67–73
20. Kabil, O., and Banerjee, R. (2014) Enzymology of $H_2S$ biogenesis, decay and signaling. *Antioxid. Redox Signal.* **20,** 770–782
21. Libiad, M., Yadav, P. K., Vitvitsky, V., Martinov, M., and Banerjee, R. (2014) Organization of the human mitochondrial hydrogen sulfide oxidation pathway. *J. Biol. Chem.* **289,** 30901–30910
22. Lagoutte, E., Mimoun, S., Andriamihaja, M., Chaumontet, C., Blachier, F., and Bouillaud, F. (2010) Oxidation of hydrogen sulfide remains a priority in mammalian cells and causes reverse electron transfer in colonocytes. *Biochim. Biophys. Acta* **1797,** 1500–1511
23. Mishanina, T. V., Libiad, M., and Banerjee, R. (2015) Biogenesis of reactive sulfur species for signaling by hydrogen sulfide oxidation pathways. *Nat. Chem. Biol.* **11,** 457–464
24. Wedmann, R., Onderka, C., Wei, S., Szijártó, I. A., Miljkovic, J. L., Mitrovic, A., Lange, M., Savitsky, S., Yadav, P. K., Torregrossa, R., Harrer, E. G., Harrer, T., Ishii, I., Gollasch, M., Wood, M. E., *et al.* (2016) Improved tag-switch method reveals that thioredoxin acts as depersulfidase and controls the intracellular levels of protein persulfidation. *Chem. Sci.* **7,** 3414–3426
25. Nicholls, P., Marshall, D. C., Cooper, C. E., and Wilson, M. T. (2013) Sulfide inhibition of and metabolism by cytochrome c oxidase. *Biochem. Soc. Trans.* **41,** 1312–1316
26. Filipovic, M. R., Miljkovic, J. Lj., Nauser, T., Royzen, M., Klos, K., Shubina, T., Koppenol, W. H., Lippard, S. J., and Ivanović-Burmazović, I. (2012) Chemical characterization of the smallest S-nitrosothiol, HSNO: cellular cross-talk of $H_2S$ and S-nitrosothiols. *J. Am. Chem. Soc.* **134,** 12016–12027
27. Miljkovic, J. Lj, Kenkel, I., Ivanović-Burmazović, I., and Filipovic, M. R. (2013) Generation of HNO and HSNO from nitrite by heme-iron-catalyzed metabolism with $H_2S$. *Angew. Chem. Int. Ed. Engl.* **52,** 12061–12064
28. Murphy, M. P. (2012) Mitochondrial thiols in antioxidant protection and redox signaling: distinct roles for glutathionylation and other thiol modifications. *Antioxid. Redox Signal.* **16,** 476–495
29. Kamoun, P., Belardinelli, M. C., Chabli, A., Lallouchi, K., and Chadefaux-Vekemans, B. (2003) Endogenous hydrogen sulfide overproduction in Down syndrome. *Am. J. Med. Genet. A* **116A,** 310–311
30. Manna, P., Gungor, N., McVie, R., and Jain, S. K. (2014) Decreased cystathionine-γ-lyase (CSE) activity in livers of type 1 diabetic rats and peripheral blood mononuclear cells (PBMC) of type 1 diabetic patients. *J. Biol. Chem.* **289,** 11767–11778
31. Tiranti, V., Viscomi, C., Hildebrandt, T., Di Meo, I., Mineri, R., Tiveron, C., Levitt, M. D., Prelle, A., Fagiolari, G., Rimoldi, M., and Zeviani, M. (2009) Loss of ETHE1, a mitochondrial dioxygenase, causes fatal sulfide toxicity in ethylmalonic encephalopathy. *Nat. Med.* **15,** 200–205

32. Yu, F., Li, P., Song, P., Wang, B., Zhao, J., and Han, K. (2012) An ICT-based strategy to a colorimetric and ratiometric fluorescence probe for hydrogen sulfide in living cells. *Chem. Commun. (Camb.)* **48,** 2852–2854
33. Lin, V. S., Lippert, A. R., and Chang, C. J. (2013) Cell-trappable fluorescent probes for endogenous hydrogen sulfide signaling and imaging $H_2O_2$-dependent $H_2S$ production. *Proc. Natl. Acad. Sci. U.S.A.* **110,** 7131–7135
34. Lord, S. J., Conley, N. R., Lee, H. L., Samuel, R., Liu, N., Twieg, R. J., and Moerner, W. E. (2008) A photoactivatable push-pull fluorophore for single-molecule imaging in live cells. *J. Am. Chem. Soc.* **130,** 9204–9205
35. Shimamoto, K., and Hanaoka, K. (2015) Fluorescent probes for hydrogen sulfide ($H_2S$) and sulfane sulfur and their applications to biological studies. *Nitric Oxide* **46,** 72–79
36. Lin, V. S., Chen, W., Xian, M., and Chang, C. J. (2015) Chemical probes for molecular imaging and detection of hydrogen sulfide and reactive sulfur species in biological systems. *Chem. Soc. Rev.* **44,** 4596–4618
37. Henthorn, H. A., and Pluth, M. D. (2015) Mechanistic insights into the $H_2S$-mediated reduction of aryl azides commonly used in $H_2S$ Detection. *J. Am. Chem. Soc.* **137,** 15330–15336
38. Chen, W., Pacheco, A., Takano, Y., Day, J. J., Hanaoka, K., and Xian, M. (2016) A single fluorescent probe to visualize hydrogen sulfide and hydrogen polysulfides with different fluorescence signals. *Angew. Chem. Int. Ed. Engl.* **55,** 9993–9996
39. Hartle, M. D., Hansen, R. J., Tresca, B. W., Prakel, S. S., Zakharov, L. N., Haley, M. M., Pluth, M. D., and Johnson, D. W. (2016) A synthetic supramolecular receptor for the hydrosulfide anion. *Angew. Chem. Int. Ed. Engl.* **55,** 11480–11484
40. Hartle, M. D., Prell, J. S., and Pluth, M. D. (2016) Spectroscopic investigations into the binding of hydrogen sulfide to synthetic picket-fence porphyrins. *Dalton Trans.* **45,** 4843–4853
41. Dufton, N., Natividad, J., Verdu, E. F., and Wallace, J. L. (2012) Hydrogen sulfide and resolution of acute inflammation: a comparative study utilizing a novel fluorescent probe. *Sci. Rep.* **2,** 499
42. Qian, Y., Zhang, L., Ding, S., Deng, X., He, C., Zheng, X. E., Zhu, H.-L., and Zhao, J. (2012) A fluorescent probe for rapid detection of hydrogen sulfide in blood plasma and brain tissues in mice. *Chem. Sci.* **3,** 2920–2923
43. Smith, R. A., Hartley, R. C., Cochemé, H. M., and Murphy, M. P. (2012) Mitochondrial pharmacology. *Trends Pharmacol. Sci.* **33,** 341–352
44. Smith, R. A., Porteous, C. M., Gane, A. M., and Murphy, M. P. (2003) Delivery of bioactive molecules to mitochondria *in vivo*. *Proc. Natl. Acad. Sci. U.S.A.* **100,** 5407–5412
45. Montoya, L. A., and Pluth, M. D. (2012) Selective turn-on fluorescent probes for imaging hydrogen sulfide in living cells. *Chem. Commun. (Camb.)* **48,** 4767–4769
46. Lippert, A. R., New, E. J., and Chang, C. J. (2011) Reaction-based fluorescent probes for selective imaging of hydrogen sulfide in living cells. *J. Am. Chem. Soc.* **133,** 10078–10080
47. Cochemé, H. M., Quin, C., McQuaker, S. J., Cabreiro, F., Logan, A., Prime, T. A., Abakumova, I., Patel, J. V., Fearnley, I. M., James, A. M., Porteous, C. M., Smith, R. A., Saeed, S., Carré, J. E., Singer, M., *et al.* (2011) Measurement of $H_2O_2$ within living *Drosophila* during aging using a ratiometric mass spectrometry probe targeted to the mitochondrial matrix. *Cell Metab.* **13,** 340–350
48. Cochemé, H. M., Logan, A., Prime, T. A., Abakumova, I., Quin, C., McQuaker, S. J., Patel, J. V., Fearnley, I. M., James, A. M., Porteous, C. M., Smith, R. A., Hartley, R. C., Partridge, L., and Murphy, M. P. (2012) Using the mitochondria-targeted ratiometric mass spectrometry probe MitoB to measure $H_2O_2$ in living *Drosophila*. *Nat. Protoc.* **7,** 946–958
49. Logan, A., Cochemé, H. M., Li Pun, P. B., Apostolova, N., Smith, R. A., Larsen, L., Larsen, D. S., James, A. M., Fearnley, I. M., Rogatti, S., Prime, T. A., Finichiu, P. G., Dare, A., Chouchani, E. T., Pell, V. R., *et al.* (2014) Using exomarkers to assess mitochondrial reactive species *in vivo*. *Biochim. Biophys. Acta* **1840,** 923–930
50. Pun, P. B., Logan, A., Darley-Usmar, V., Chacko, B., Johnson, M. S., Huang, G. W., Rogatti, S., Prime, T. A., Methner, C., Krieg, T., Fearnley, I. M., Larsen, L., Larsen, D. S., Menger, K. E., Collins, Y., *et al.* (2014) A mitochondria-targeted mass spectrometry probe to detect glyoxals: implications for diabetes. *Free Radic. Biol. Med.* **67,** 437–450
51. Ono, H., and Ito, A. (1984) Transport of the precursor for sulfite oxidase into intermembrane space of liver mitochondria: characterization of import and processing activities. *J. Biochem.* **95,** 345–352
52. Artaud, I., and Galardon, E. (2014) A persulfide analogue of the nitrosothiol SNAP: formation, characterization and reactivity. *ChemBioChem* **15,** 2361–2364
53. Yadav, P. K., Martinov, M., Vitvitsky, V., Seravalli, J., Wedmann, R., Filipovic, M. R., and Banerjee, R. (2016) Biosynthesis and reactivity of cysteine persulfides in signaling. *J. Am. Chem. Soc.* **138,** 289–299
54. Asin-Cayuela, J., Manas, A. R., James, A. M., Smith, R. A., and Murphy, M. P. (2004) Fine-tuning the hydrophobicity of a mitochondria-targeted antioxidant. *FEBS Lett.* **571,** 9–16
55. Dare, A. J., Bolton, E. A., Pettigrew, G. J., Bradley, J. A., Saeb-Parsy, K., and Murphy, M. P. (2015) Protection against renal ischemia-reperfusion injury *in vivo* by the mitochondria targeted antioxidant MitoQ. *Redox. Biol.* **5,** 163–168
56. Dare, A. J., Logan, A., Prime, T. A., Rogatti, S., Goddard, M., Bolton, E. M., Bradley, J. A., Pettigrew, G. J., Murphy, M. P., and Saeb-Parsy, K. (2015) The mitochondria-targeted anti-oxidant MitoQ decreases ischemia-reperfusion injury in a murine syngeneic heart transplant model. *J. Heart Lung Transplant.* **34,** 1471–1480
57. Barca, E., Kleiner, G., Tang, G., Ziosi, M., Tadesse, S., Masliah, E., Louis, E. D., Faust, P., Kang, U. J., Torres, J., Cortes, E. P., Vonsattel, J. P., Kuo, S. H., and Quinzii, C. M. (2016) Decreased coenzyme Q10 levels in multiple system atrophy cerebellum. *J. Neuropathol. Exp. Neurol.* **75,** 663–672
58. Yadav, P. K., Yamada, K., Chiku, T., Koutmos, M., and Banerjee, R. (2013) Structure and kinetic analysis of $H_2S$ production by human mercaptopyruvate sulfurtransferase. *J. Biol. Chem.* **288,** 20002–20013
59. Porteous, C. M., Logan, A., Evans, C., Ledgerwood, E. C., Menon, D. K., Aigbirhio, F., Smith, R. A., and Murphy, M. P. (2010) Rapid uptake of lipophilic triphenylphosphonium cations by mitochondria in vivo following intravenous injection: implications for mitochondria-specific therapies and probes. *Biochim. Biophys. Acta* **1800,** 1009–1017
60. Porteous, C. M., Menon, D. K., Aigbirhio, F. I., Smith, R. A., and Murphy, M. P. (2013) P-glycoprotein (Mdr1a/1b) and breast cancer resistance protein (Bcrp) decrease the uptake of hydrophobic alkyl triphenylphosphonium cations by the brain. *Biochim. Biophys. Acta* **1830,** 3458–3465
61. Denekamp, C., Pocsfalvi, G., and Claeys, M. (1999) Charge-remote and charge-proximate fragmentations in deuterium-labeled *n*-hexyadecyltriphenylphosphonium cations. *Int. J. Mass Spectrom.* **188,** 163–175
62. Chouchani, E. T., Pell, V. R., Gaude, E., Aksentijević, D., Sundier, S. Y., Robb, E. L., Logan, A., Nadtochiy, S. M., Ord, E. N., Smith, A. C., Eyassu, F., Shirley, R., Hu, C. H., Dare, A. J., James, A. M., *et al.* (2014) Ischaemic accumulation of succinate controls reperfusion injury through mitochondrial ROS. *Nature* **515,** 431–435
63. Chouchani, E. T., Pell, V. R., James, A. M., Work, L. M., Saeb-Parsy, K., Frezza, C., Krieg, T., and Murphy, M. P. (2016) A unifying mechanism for mitochondrial superoxide production during ischemia-reperfusion injury. *Cell Metab.* **23,** 254–263
64. Beckman, J. S., Beckman, T. W., Chen, J., Marshall, P. A., and Freeman, B. A. (1990) Apparent hydroxyl radical production by peroxynitrite: implications for endothelial injury from nitric oxide and superoxide. *Proc. Natl. Acad. Sci. U.S.A.* **87,** 1620–1624
65. Hughes, M. N., and Nicklin, H. G. (1968) The chemistry of pernitrites: part 1. kinetics of decomposition of pernitrous acid. *J. Am. Chem. Soc. A* **1968,** 450–452
66. Cline, J. D. (1969) Spectrophotometric determination of hydrogen sulfide in natural waters. *Limnology Oceanography* **14,** 454–458
67. Gornall, A. G., Bardawill, C. J., and David, M. M. (1949) Determination of serum protein by means of the biuret reaction. *J. Biol. Chem.* **177,** 751–766
68. Corry, R. J., Winn, H. J., and Russell, P. S. (1973) Heart transplantation in congenic strains of mice. *Transplant. Proc.* **5,** 733–735
69. Schmidt, B., Metzner, A., Chun, K. R., Leftheriotis, D., Yoshiga, Y., Fuernkranz, A., Neven, K., Tilz, R. R., Wissner, E., Ouyang, F., and Kuck, K. H. (2010) Feasibility of circumferential pulmonary vein isolation using a novel endoscopic ablation system. *Circ. Arrhythm. Electrophysiol.* **3,** 481–488

**Supplementary Information**

# Assessment of $H_2S$ *in vivo* using the recently developed mitochondria-targeted mass spectrometry probe MitoA

Sabine Arndt[a], Carlos D. Baeza-Garza[b], Angela Logan[a], Tiziana Rosa[c], Rudolf Wedmann[d], Tracy A. Prime[a], Jack L. Martin[e], Kourosh Saeb-Parsey[e], Thomas Krieg[c], *Milos*. R. Filipovic[d], Richard C. Hartley[b,*], and Michael P. Murphy[a,*]

[a]MRC Mitochondrial Biology Unit, Hills Road, Cambridge CB2 0XY, UK.
[b]WestCHEM School of Chemistry, University of Glasgow, Glasgow G12 8QQ, UK.
[c]Department of Medicine, University of Cambridge, Addenbrooke's Hospital, Hills Road, Cambridge, CB2 2QQ, UK.
[d]University of Bordeaux, IBGC, UMR 5095, F-33077 Bordeaux, France; 3 CNRS, IBGC, UMR 5095, F-33077 Bordeaux, France
[e]Department of Surgery and Cambridge NIHR Biomedical Research Centre, Biomedical Campus, University of Cambridge, Addenbrooke's Hospital, Hills Road, Cambridge, CB2 2QQ, UK.

**A**

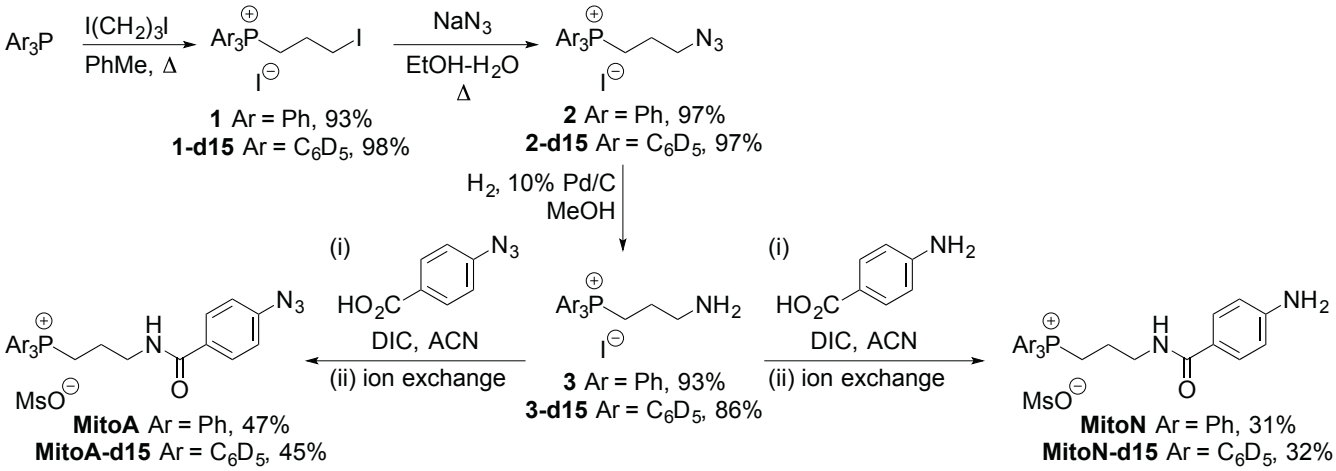


**B**

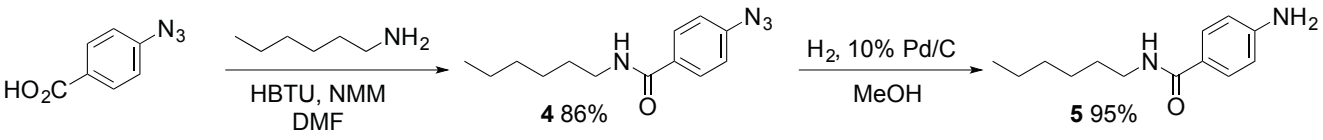


Fig. S1 (A) Synthesis of MitoA and MitoN. ACN = acetonitrile, DIC = *N, N'*-diisopropylcarbodiimide. (B) Control compounds **4** and **5** lacking the TPP targeting group were also prepared.Coupling of hexylamine with 4-azidobenzoic acid was achieved using *N,N,N′,N′*-tetramethyl-*O*-(1*H*-benzotriazol-1-yl)uronium hexafluorophosphate (HBTU) to give amide **4**, which was then hydrogenated to give the amine **5**.

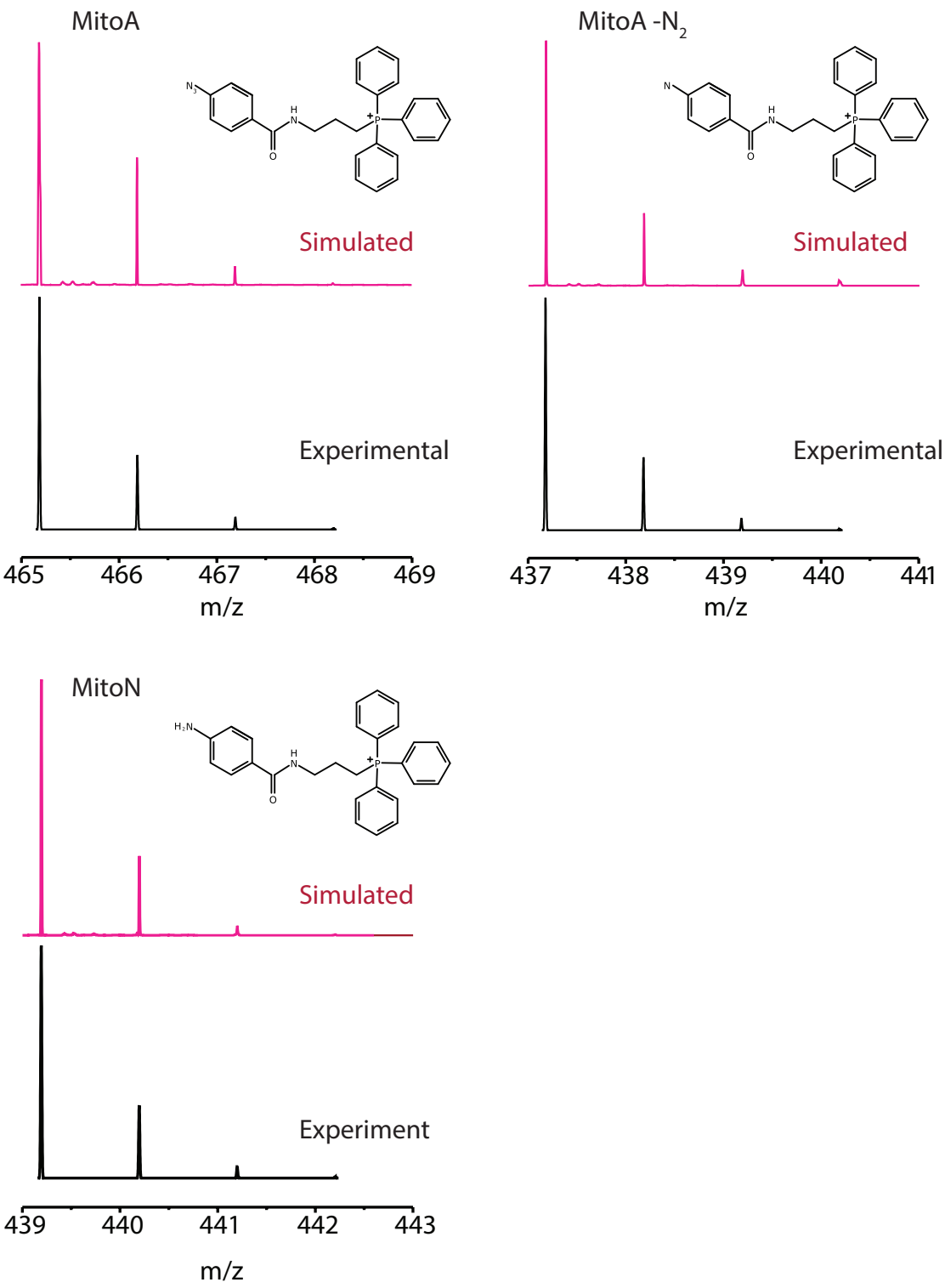


Fig. S2 Mass spectra of MitoA and MitoN. Observed (black) and simulated peaks (pink) for: MitoA, $[C_{28}H_{26}N_4OP]^+$ predicted m/z 465.1839. MitoA nitrene decomposition product from $N_2$ neutral loss $[C_{28}H_{26}N_2OP]^+$ predicted m/z 437.1782 MitoN, $[C_{28}H_{29}N_2OP]^+$ predicted m/z 439.1934.Spectra were obtained using an ultra-high resolution electron spray time of flight mass spectrometer (maXis Bruker Daltonics).

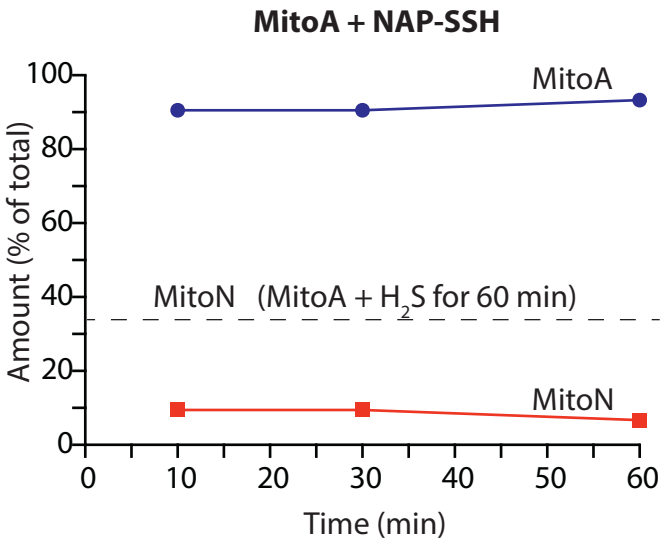


Fig. S3 Reactivity of MitoA with a persulfide. MitoA (10 μM) was mixed with NAP-SSH (25 μM) in KCl buffer, pH 7.2 at 37 °C. Samples were taken at the indicated times and analysed by RP-HPLC. The amounts of MitoA and MitoN were determined by RP-HPLC from standard curves and used to calculate the amount of that compound as a percentage of the sum of MitoA and MitoN. The dashed line shows the amount of MitoN formed by incubating MitoA (10 μM) $NaS_2$ (25 μM) in KCl buffer, pH 7.2 at 37 °C for 60 min.

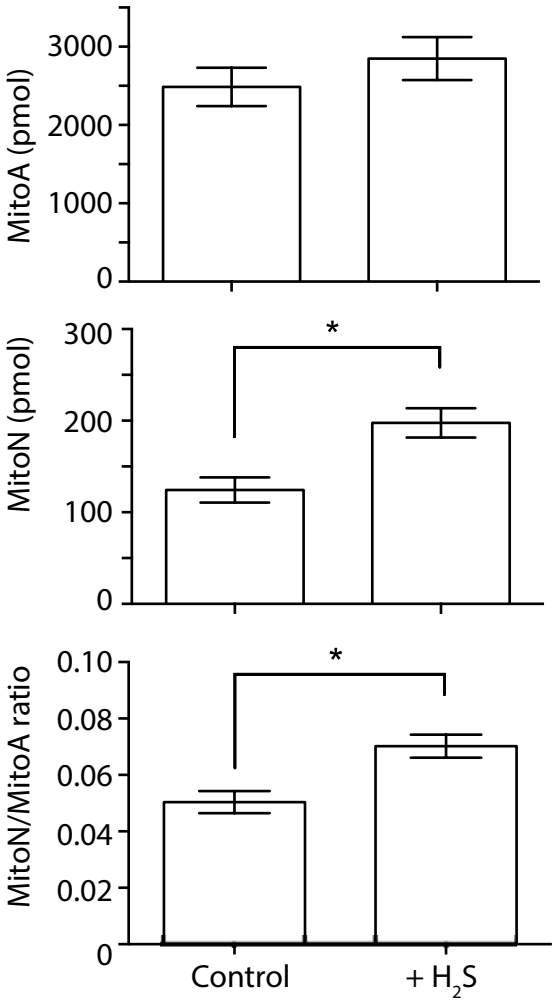


Fig. S4 Reactivity of MitoA with $H_2S$ during extraction for mass spectrometry
MitoA (10 µM) was incubated with NaHS (10 µM) for 4 h in 95 % ACN. After the incubation, samples were dried under vacuum, resuspended in 20 % ACN, 0.1 % FA with internal standards and the amounts of MitoA, MitoN and the MitoN/MitoA ratio were quantified by LC-MS/MS. Data are means ± SEM, n = 4. *$p < 0.05$; two-tailed t-test.

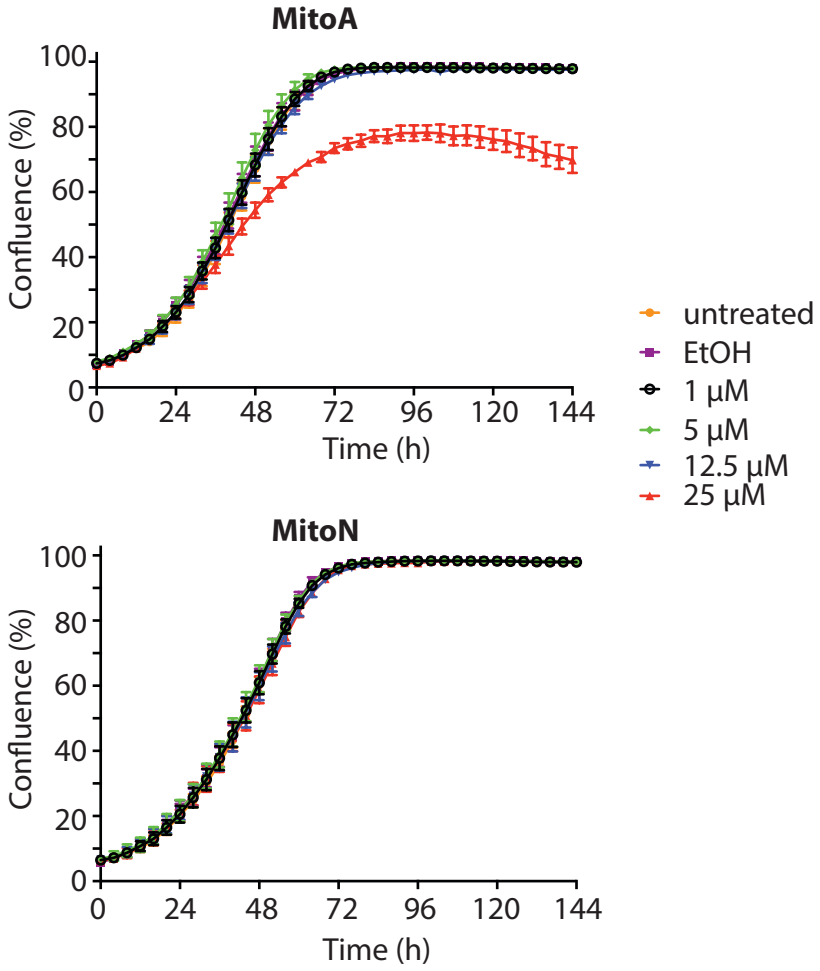


Fig. S5 Effect of MitoA and MitoN on cell proliferation. C2C12 cells were plated at 10,000 cells per well in 6-well plates (~1 000 cells per $cm^2$) and treating with MitoA or MitoN.Cell proliferation was then monitored by measuring confluency via automated bright field imaging (IncuCyte HD, EssenBioScience) for 144 h. Data are means ± SEM, n = 3.

## Supplementary Experimental Procedures

### *Chemical syntheses*

All reactions under an inert atmosphere were carried out using oven-dried or flame-dried glassware and solvents were added via syringe. Reagents were obtained from commercial suppliers and used without further purification. Dry solvents were collected from a Puresolv solvent purification system, obtained from commercial suppliers or dried in the laboratory. Ethanol was distilled from Mg turnings activated with iodine. $^{1}$H NMR spectra were obtained using Bruker DPX/400 and Bruker-Avance III spectrometers operating at 400 and 500 MHz, $^{13}$C NMR spectra at 101 and 126 MHz respectively. Signal splitting patterns were described as: singlet (s), doublet (d), triplet (t), quartet (q), multiplet (m), broad singlet (s, broad), or any combination of the above. All coupling constants were recorded in Hz. DEPT was used to assign the signals in $^{13}$C NMR spectra as C, CH, $CH_2$ and $CH_3$.

*(3-Iodopropyl)triphenylphosphonium iodide* (**1**)

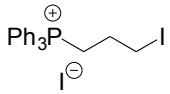

1,3-Diiodopropane (2.65 mL, 23 mmol) was added to a stirred solution of triphenylphosphine (3.01 g, 11.5 mmol) in toluene (25 mL) at 95 °C and the mixture was stirred for 20 h under reflux. After cooling to RT, the precipitate was collected by filtration and washed with $Et_2O$, after this, it was dried under reduced pressure to yield the alkyl iodide **1** as a white amorphous solid. (5.98 g, 93%). Mp: 172-174 °C. $\nu_{max}$ (ATR): 3056 (CH), 2916 (CH), 2849 (CH), 1587 (Ar). $\delta_H$ ($CDCl_3$, 400 MHz): 7.81-7.76 (9H, m, 6 *o*-H $PPh_3$, 3 *p*-H $PPh_3$), 7.71-7.66 (6H, m, 6 *m*-H $PPh_3$), 3.92-3.84 (2H, m, P-$CH_2$), 3.56 (2H, t, $J$ = 6.4 Hz, I-$CH_2$), 2.19-2.10 (2H, m, $CH_2$-*$CH_2$*-$CH_2$). $\delta_C$ ($CDCl_3$, 125 MHz): 135.61 (d, $J$ = 2.8 Hz, CH), 134.00 (d, $J$ = 10.1 Hz, CH), 130.93 (d, $J$ = 12.8 Hz, CH), 118.01 (d, $J$ = 86.1 Hz, C), 27.08 (d, $J$ = 1.8 Hz, $CH_2$), 24.41 (d, $J$ = 51.3 Hz, $CH_2$), 6.96 (d, $J$ = 20.1 Hz, $CH_2$). LRMS (ESI$^+$) 431 [$M^+$ (phosphonium cation), 100%]. HRMS (ESI$^+$): 430.9137. $C_{21}H_{21}IP$ requires $M^+$ (phosphonium cation), 430.9117.

*(3-Iodoprop-1-yl)-tri(pentadeuterophenyl)phosphonium iodide* (***$d_{15}$*-1**)

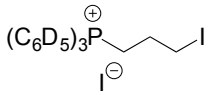

1,3-Diiodopropane (500 μL, 4.3 mmol) was added to a stirring solution of d-15 triphenylphosphine (500 mg, 1.8 mmol) in toluene (10 mL) at 95 °C and the mixture was set to react for 20 h under reflux conditions. After cooling to RT, the precipitate was collected by filtration and washed with $Et_2O$, after this, it was dried under reduced pressure to yield the alkyl iodide ***$d_{15}$*-1** as a white amorphous solid. (1.01 g, 98%). Mp: 173-175 °C. $\nu_{max}$ (ATR): 2859 (CH), 2343 (CD), 1559 (Ar). $\delta_H$ ($CDCl_3$, 500 MHz): 3.97-3.91 (2H, m, P-$CH_2$), 3.60 (2H, t, $J$ = 6.5, I-$CH_2$), 2.21-2.14 (2H, m, $CH_2$-*$CH_2$*-$CH_2$). $\delta_C$ ($CDCl_3$, 125 MHz): 135.11-134.73 (m, CD), 133.65-133.16 (m, CD), 130.50-129.99 (m, CD), 117.2 (d, $J$ = 86.2 Hz, C), 26.90 (d, $J$ = 2.0 Hz, $CH_2$), 24.24 (d, $J$ = 51.2 Hz, $CH_2$), 6.77 (d, $J$ = 20.0 Hz, $CH_2$). LRMS (ESI$^+$) 446 [$M^+$ (phosphonium cation), 100%] HRMS (ESI$^+$): 446.1351. $C_{21}H_6D_{15}IP$ requires $M^+$ (phosphonium cation), 446.1362.

*(3-Azidoprop-1-yl)triphenylphosphonium iodide* (**2**)

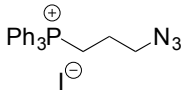

A solution of (3-iodoprop-1-yl)triphenylphosphonium iodide **1** (5.02 g, 9.0 mmol) and $NaN_3$ (1.17 g, 18.0 mmol) in EtOH (15.0 mL) and $H_2O$ (15.0 mL) was stirred and heated to 70 °C for 24 h. After cooling, an extraction was carried out with $CHCl_3$ (3 30 mL). The combined organic layers were dried over $MgSO_4$, filtered and concentrated under reduced pressure to yield the alkyl azide **2** as an amorphous beige solid (4.13 g, 97%). MP: 151-153 °C $\delta_H$ ($CDCl_3$, 400 MHz): 7.85-7.79 (9H, m, 6 *o*-H $PPh_3$, 3 *p*-H $PPh_3$), 7.73-7.68 (6H, m, 6 *m*-H $PPh_3$), 3.95-3.87 (2H, m, P-$CH_2$), 3.82 (2H, t, $J$ = 6.2 Hz, $N_3$-$CH_2$), 1.95-1.86 (2H, m, $CH_2$-*$CH_2$*-$CH_2$). $\delta_C$ ($CDCl_3$, 100 MHz): 135.57 (d, $J$ = 2.9 Hz, CH), 133.95 (d, $J$ = 10.3 Hz, CH), 130.92 (d, $J$ = 12.5 Hz, CH), 118.05 (d, $J$ = 86.6 Hz, C), 50.98 (d, $J$ = 17.6 Hz, $CH_2$), 22.92 (d, $J$ = 2.9 Hz, $CH_2$), 20.70 (d, $J$ = 52.8 Hz, $CH_2$). $^1$H and $^{13}$C NMR data agree with those for the bromide salt [1].

*(3-Azidoprop-1-yl)-tri(pentadeuterophenyl)phosphonium iodide* (***d*$_{15}$-2**)

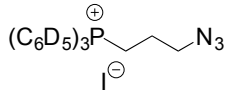

A solution of alkyl iodide ***d*$_{15}$-1** (1.00 g, 1.74 mmol) and $NaN_3$ (260 mg, 4.0 mmol) in EtOH (5.0 mL) and $H_2O$ (5.0 mL) was stirred and heated to 70 °C for 24 h. After cooling, an extraction was carried out with DCM (3 30 mL). The combined organic layers were dried over $MgSO_4$, filtered and concentrated under reduced pressure to yield the alkyl azide ***d*$_{15}$-2** as an amorphous beige solid (825 mg, 97%). Mp: 151-153 °C. $\nu_{max}$ (ATR): 2888 (CH), 2796 (CH), 2362 (CD), 2110 ($N_3$), 1546 (Ar). $\delta_H$ ($CDCl_3$, 500 MHz): 3.83-3.76 (4H, m, P-$CH_2$, $N_3$-$CH_2$), 1.91-1.83 (2H, m, $CH_2$-*$CH_2$*-$CH_2$). $\delta_C$ ($CDCl_3$, 125 MHz): 134.99-134.60 (m, CD), 133.47-132.98 (m, CD), 130.40-129.91 (m, CD), 117.40 (d, $J$ = 86.2 Hz, C), 50.71 (d, $J$ = 17.5 Hz, $CH_2$), 22.63 (d, $J$ = 2.6 Hz, $CH_2$), 20.33 (d, $J$ = 52.9 Hz, $CH_2$). LRMS (ESI$^+$) 361 [$M^+$ (phosphonium cation), 34%], 333 [$M^+$ (phosphonium cation) – $N_2$, 100%]. HRMS (ESI$^+$): 361.2395. $C_{21}H_6D_{15}N_3P$ requires $M^+$ (phosphonium cation), 361.2409.

*(3-Aminoprop-1-yl)triphenylphosphonium iodide* (**3**)

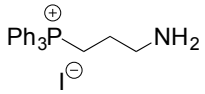

A solution of alkyl azide **2** (4.10 g, 8.7 mmol) and 10% Pd/C (425 mg, 4.0 mmol) in MeOH (40 mL) was stirred at RT under a $H_2$ (1 atm) atmosphere for 6 h. After this time, the mixture was filtered through Celite®. Then, the mixture was concentrated under reduced pressure to yield the amine **3** as an amorphous beige solid (3.62 g, 93%). Mp: 212-214 °C. $\nu_{max}$ (ATR): 3050 (NH), 2887 (CH), 2789 (CH), 1586 (Ar). $\delta_H$ ($CDCl_3$, 400 MHz): 7.83-7.76 (9H, m, 6 *o*-H $PPh_3$, 3 *p*-H $PPh_3$), 7.71-7.66 (6H, m, 6 *m*-H $PPh_3$), 3.78-3.71 (2H, m, P-$CH_2$), 3.01 (2H, t, $J$ = 6.2 Hz, $NH_2$-*$CH_2$*), 1.88 (2H, s, $NH_2$), 1.82-1.72 (2H, m, $CH_2$-*$CH_2$*-$CH_2$). $\delta_C$ ($CDCl_3$, 100 MHz): 135.38 (d, $J$ = 2.9 Hz, CH), 133.99 (d, $J$ = 9.7 Hz, CH), 130.84 (d, $J$ = 12.6 Hz, CH), 118.48 (d, $J$ = 85.5 Hz, C), 41.74 (d, $J$ = 17.5 Hz, $CH_2$), 26.13 (d, $J$ = 4.9 Hz, $CH_2$), 21.14 (d, $J$ = 51.5 Hz,

$CH_2$). LRMS ($ESI^+$) 320 [$M^+$ (phosphonium cation), 100%], HRMS ($ESI^+$): 320.1553. $C_{21}H_{23}NP$ requires $M^+$ (phosphonium cation), 320.1563.

*(3-Aminopropyl)-tri(pentadeuterophenyl)phosphonium iodide* (*$d_{15}$*-**3**)

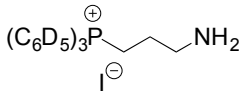

A solution of alkyl azide *$d_{15}$*-**2** (820 mg, 1.68 mmol) and 10% Pd/C (100 mg, 0.94 mmol) in MeOH (10 mL) was stirred at RT under a $H_2$ (1 atm) atmosphere for 6 h. After this time, the mixture was filtered through Celite®. Then, the mixture was concentrated under reduced pressure to yield the amine *$d_{15}$*-**3** as an amorphous beige solid (671 mg, 86%). Mp: 211-213 °C. $\nu_{max}$ (ATR): 2950 (NH), 2887 (CH), 2789 (CH), 2251 (CD), 1547 (Ar). $\delta_H$ ($CDCl_3$, 400 MHz): 3.79-3.72 (2H, m, P-$CH_2$), 3.01 (2H, t, $J$ = 6.3 Hz, $NH_2$-*$CH_2$*), 1.80-1.71 (2H, m, $CH_2$-*$CH_2$*-$CH_2$), 1.48 (2H, s, $NH_2$). $\delta_C$ ($CDCl_3$, 100 MHz): 135.04-134.48 (m, CD), 133.70-133.09 (m, CD), 130.50-129.84 (m, CD), 118.15 (d, $J$ = 85.7 Hz, C), 41.65 (d, $J$ = 17.5 Hz, $CH_2$), 26.18 (d, $J$ = 2.5 Hz, $CH_2$), 21.01 (d, $J$ = 52.7 Hz, $CH_2$). LRMS ($ESI^+$) 335 [$M^+$ (phosphonium cation), 100%]. HRMS ($ESI^+$): 335.2489. $C_{21}H_8D_{15}NP$ requires $M^+$ (phosphonum cation), 335.2504.

*[3-(4'-Azidobenzamido)-prop-1-yl]triphenylphosphonium mesylate* (**MitoA**, mesylate salt)

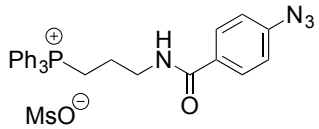

A solution of **3** (2.24 g, 5.0 mmol), 4-azidobenzoic acid (816 mg, 5.0 mmol), and *N, N'*-diisopropylcarbodiimide (800 µl, 5.2 mmol) in dry ACN (20 mL) was stirred at RT under argon for 48 h. After this, the precipitate was washed with ACN (5 × 10 mL). The precipitate was dried under high vacuum to remove the solvent, resulting in a brown powder. The powder was then treated for ion exchange with ion exchange resin Araldite® IRA-400 charged with mesylate ions giving a brown amorphous solid after solvent was removed. Column chromatography [$SiO_2$, DCM-MeOH (95:5)] yielded the mesylate salt of **MitoA** as a brown amorphous solid (1.34 g, 47%). $R_f$ [$SiO_2$, DCM-MeOH (95:5)]: 0.25. Mp: 157-159 °C. $\nu_{max}$ (ATR): 3289 (NH), 3063 (CH), 2928 (CH), 2901 (CH), 2120 ($N_3$), 1653 (C=O), 1601 (Ar), 1530 (Ar), 1497 (Ar) $cm^{-1}$. $\delta_H$ ($CDCl_3$, 400 MHz): 9.28 (t, $J$ = 5.9 Hz, NH), 8.15 (2H, d, $J$ = 8.9 Hz, H-2', H-6'), 7.76-7.69 (9H, m, 3 × *p*-H $PPh_3$, 6 x *o*-H $PPh_3$), 7.64 – 7.59 (6H, m, 6 *m*-H $PPh_3$), 7.07 (2H, d, $J$ = 8.8 Hz, H-3', H-5'), 3.75-3.67 (4H, m, P-*$CH_2$*, NH-*$CH_2$*), 2.81 (3H, s, *$CH_3SO_3^-$*), 1.98-1.90 (2H, m, $CH_2$-*$CH_2$*-$CH_2$). $\delta_C$ ($CDCl_3$, 100 MHz): 167.10 (C), 142.99 (C), 135.13 (d, $J$ = 2.0 Hz, CH), 133.57 (d, $J$ = 9.1 Hz, CH), 130.91 (C), 130.61 (d, $J$ = 12.0 Hz, CH), 129.81 (CH), 118.92 (CH), 118.56 (d, $J$ = 86.0 Hz, C), 39.78 ($CH_3$), 39.42 (d, $J$ = 17.0 Hz, $CH_2$), 22.60 (d, $J$ = 4.0 Hz, $CH_2$), 20.16 (d, $J$ = 52.1 Hz, $CH_2$). LRMS ($ESI^+$) 465 [$M^+$ (phosphonium cation), 32%], 437 [$M^+$ (phosphonium cation) – $N_2$, 100]. HRMS ($ESI^+$): 465.1821. $C_{28}H_{26}N_4OP$ requires $M^+$ (phosphonum cation), 465.1839

*[3-(4'-Azidobenzamido)propyl]tri(pentadeuterophenyl)phosphonium mesylate* (***d*$_{15}$-MitoA** mesylate salt)

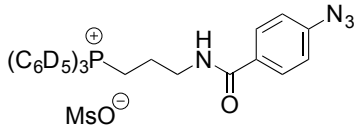

A solution of amine ***d*$_{15}$-3** (100 mg, 0.22 mmol), 4-azidobenzoic acid (36 mg, 0.22 mmol), and *N, N'*-diisopropylcarbodiimide (150 µl, 0.98 mmol) in dry ACN (2.5 mL) was stirred at RT under argon for 37 h. After this, the precipitate was washed with ACN (4 × 10 mL). The precipitate was dried under high vacuum to remove the solvent, resulting in a brown powder. The powder was then treated for ion exchange with ion exchange resin Araldite® IRA-400 charged with mesylate ions giving a brown amorphous solid after solvent was removed. Column chromatography [$SiO_2$, DCM-MeOH (95:5)] yielded the target compound as a brown amorphous solid (57 mg). As the mesylate ion was under integrated in the NMR, the solid was treated with aqueous $NaMeSO_3$ (0.5 M) and extracted with DCM. The DCM was removed under reduced pressure to give the mesylate salt of ***d*$_{15}$-MitoA** as a hygroscopic thick yellow oil (55 mg, 45%). $R_f$[$SiO_2$, DCM-MeOH (95:5)]: 0.27. Mp: 156-158 °C. $\nu_{max}$ (ATR): 3283 (NH), 2935 (CH), 2906 (CH), 2823 (CH), 2269 (CD), 2120 ($N_3$), 1644 (C=O), 1603 (Ar), 1546 (Ar), 1500 (Ar). $\delta_H$ ($CDCl_3$, 400 MHz): 9.10-9.08 (1H, m, NH), 7.98 (2H, d, *J* = 8.6 Hz, H-2', H-6'), 6.86 (2H, d, *J* = 8.6 Hz, H-3', H-5'), 3.53-3.46 (4H, m, P-*$CH_2$*, NH-*$CH_2$*), 2.57 (3H, s, *$CH_3SO_3^-$*), 1.83-1.81 (2H, m, $CH_2$-*$CH_2$*-$CH_2$). δ ($CDCl_3$, 100 MHz): 166.40 (C), 142.34 (C), 134.51-134.04 (m, CD), 132.96-132.36 (m, CD), 130.41 (C), 130.01-129.41 (m, CD), 129.31 (CH), 118.40 (CH), 117.66 (d, *J* = 86.1 Hz, C), 39.29 ($CH_3$), 39.06 (d, *J* = 17.0 Hz, $CH_2$), 22.14 (d, *J* = 4.1 Hz, $CH_2$), 19.66 (d, *J* = 52.3 Hz, $CH_2$). LRMS ($ESI^+$) 480 [$M^+$ (phosphonium cation), 30%], 452 [$M^+$ (phosphonium cation) – $N_2$, 100]. HRMS ($ESI^+$): 480.2760. $C_{28}H_{11}D_{15}N_4OP^+$ requires $M^+$ (phosphonum cation), 480.2780

*[3-(4'-Aminobenzamido)prop-1-yl]triphenylphosphonium mesylate* (**MitoN** mesylate salt).

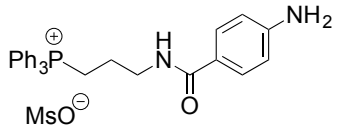

A solution of amine **3** (1.12 g, 2.50 mmol), 4-aminobenzoic acid (340 mg, 2.47 mmol), and *N, N'*-diisopropylcarbodiimide (400 µl, 2.68 mmol) in dry ACN (10 mL) was stirred at RT under argon for 48 h. After this, the precipitate was washed with ACN (5 × 10 mL). The precipitate was dried under high vacuum to remove the solvent, resulting in a beige powder. The powder was then treated for ion exchange with ion exchange resin Araldite® IRA-400 charged with mesylate ions giving a beige amorphous solid after solvent was removed. Column chromatography [$SiO_2$, DCM-MeOH (9:1)] yielded the mesylate salt of **MitoN** as a beige amorphous solid (410 mg, 31%). $R_f$[$SiO_2$, DCM-MeOH (9:1)]: 0.25. Mp: 206-208 °C. $\nu_{max}$ (ATR): 3333 (NH), 3225 (CH), 3059 (CH), 2931 (CH), 2904 (CH), 1628 (CO), 1603 (Ar), 1545 (Ar), 1508 (Ar). $\delta_H$ ($CDCl_3$, 400 MHz): 8.92 (t, *J* = 5.9 Hz, NH), 7.93 (2H, d, *J* = 8.6 Hz, H-2', H-6'), 7.76-7.68 (9H, m, 3 × *p*-H $PPh_3$, 6 × *o*-H $PPh_3$), 7.63 – 7.59 (6H, m, 6 × *m*-H $PPh_3$), 6.66 (2H, d, *J* = 8.5 Hz, H-3', H-5'), 4.07 (2H, s, $NH_2$) 3.74-3.67 (4H, m, P-*$CH_2$*, NH-*$CH_2$*), 2.83 (3H, s, *$CH_3SO_3^-$*), 1.97-1.88 (2H, m, $CH_2$-*$CH_2$*-

$CH_2$). $\delta_C$ ($CDCl_3$, 100 MHz): 167.74 (C), 149.59 (C), 134.92 (d, *J* = 2.3 Hz, CH), 133.41 (d, *J* = 9.0 Hz, CH), 130.42 (d, *J* = 12.5 Hz, CH), 129.47 (C), 123.71 (CH), 118.46 (d, *J* = 86.0 Hz, C), 114.07 (CH), 39.65 ($CH_3$), 39.06 (d, *J* = 17.0 Hz, $CH_2$), 22.64 (d, *J* = 3.0 Hz, $CH_2$), 19.79 (d, *J* = 52.0 Hz, $CH_2$). LRMS ($ESI^+$) 439 [$M^+$ (phosphonium cation), 100%]. HRMS ($ESI^+$): 439.1915. $C_{28}H_{28}N_2OP$ requires $M^+$ (phosphonum cation), 439.1934.

*[3-(4'-Aminobenzamido)prop-1-yl]tri(pentadeuterophenyl)phosphonium mesylate* (***d*$_{15}$-MitoN** mesylate salt)

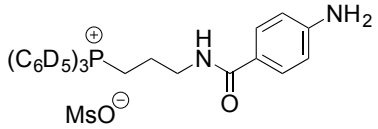


A solution of amine ***d*$_{15}$-3** (100 mg, 0.22 mmol), 4-aminobenzoic acid (30 mg, 0.21 mmol), and *N, N'*-diisopropylcarbodiimide (150 µl, 0.98 mmol) in dry ACN (2.5 mL) was stirred at RT under argon for 48 h. After this, the precipitate was washed with ACN (5 × 10 mL). The precipitate was dried under high vacuum to remove the solvent, resulting in a beige powder. The powder was then treated for ion exchange with ion exchange resin Araldite® IRA-400 charged with mesylate ions giving a beige amorphous solid after solvent was removed. Column chromatography [$SiO_2$, DCM-MeOH (9:1)] yielded the amide ***d*$_{15}$-MitoN** as a beige amorphous solid (50 mg, 42%). As the mesylate ion was under integrated in the NMR, the solid was treated with aqueous $NaMeSO_3$ (0.5 M) and extracted with DCM. The DCM was removed under reduced pressure to give the mesylate salt of ***d*$_{15}$-MitoN** as a beige solid (38 mg, 32%). $R_f$[$SiO_2$, DCM-MeOH (9:1)]: 0.25. Mp: 207-209 °C. $\nu_{max}$ (ATR): 3335 (NH), 3228 (CH), 2931 (CH), 2902 (CH), 2281 (CD), 1623 (CO), 1599 (Ar), 1549 (Ar), 1509 (Ar). $\delta_H$ ($CD_3OD$, 400 MHz): 7.56 (2H, d, *J* = 8.8 Hz, H-2', H-6'), 6.62 (2H, d, *J* = 8.8 Hz, H-3', H-5'), 3.50-3.38 (4H, m, P-*$CH_2$*, NH-*$CH_2$*), 2.65 (3H, s, *$CH_3SO_3$*), 1.96-1.86 (2H, m, $CH_2$-*$CH_2$*-$CH_2$). $\delta_C$ $CD_3OD$, (100 MHz): 170.54 (C), 153.45 (C), 136.06-135.57 (m, CD), 134.64-134.05 (m, CD), 131.37-130.74 (m, CD), 130.02 (C), 122.54 (CH), 119.54 (d, *J* = 86.4 Hz, C), 114.65 (CH), 40.78 (d, *J* = 19.0 Hz, $CH_2$), 39.52 ($CH_3$), 23.99 (d, *J* = 3.7 Hz, $CH_2$), 20.68 (d, *J* = 53.0 Hz, $CH_2$). LRMS ($ESI^+$) 454 [$M^+$ (phosphonium cation), 100%]. HRMS (ESI): 454.2855. $C_{28}H_{13}D_{15}N_2OP$ requires $M^+$ (phosphonum cation), 454.2875

*4'-Azido-N-(hex-1-yl)benzamide* (**4**)

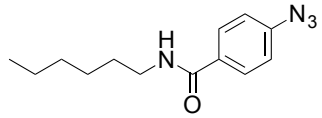


Hex-1-ylamine (320 µL, 2.4 mmol), HBTU (835 mg, 2.2 mmol), and *N*-methylmorpholine (NMM, 440 µL, 4 mmol) were added to a stirred solution of *para*-azidobenzoic acid (367 mg, 2.2 mmol) in anhydrous DMF (10 mL) at RT under argon. Stirring was continued for 18 h, and then water (15 mL) was added. The precipitate was collected by filtration and washed with water (3 × 10 mL). The resulting solid was dried under high vacuum to give the amide **4** as an amorphous yellow solid (427 mg, 86%). Mp: 71-73 °C. $\nu_{max}$ (ATR): 3312 (NH), 3075 (CH), 2955 (CH), 2928 (CH), 2860 (CH), 2137 ($N_3$), 1629 (CO), 1605 (Ar), 1545 (Ar), 1499 (Ar). $\delta_H$ ($CDCl_3$, 500 MHz): 7.76 (2H, d, *J* = 8.6 Hz, H-2', H-6'), 7.05 (2H, d, *J* = 8.6 Hz, H-3', H-5'), 6.14 (1H, s, NH), 3.45-3.41 (2H, m, $CH_2$-1), 1.60 (2H, qn, *J* = 7.0

Hz, $CH_2$-2), 1.40-1.28 (6H, m, $CH_2$-3, $CH_2$-4, and $CH_2$-5), 0.91-0.87 (3H, t, $J$ = 7.0 Hz, $CH_3$). $\delta_C$ ($CDCl_3$, 125 MHz): 166.57 (C), 143.30 (C), 131.53 (C), 128.78 (CH), 119.03 (CH), 40.32 ($CH_2$), 31.65 ($CH_2$), 29.78 ($CH_2$), 26.82 ($CH_2$), 22.69 ($CH_2$), 14.16 ($CH_3$). LRMS ($EI^+$): 246 ($M^{+\bullet}$, 47%), 218 ($M^{+\bullet} - N_2$, 100%), HRMS ($EI^+$): 246.1483. $C_{13}H_{18}N_4O$ requires $M^{+\bullet}$, 246.1481.

*4'-Amino-N-(hex-1-yl)benzamide* (**5**)

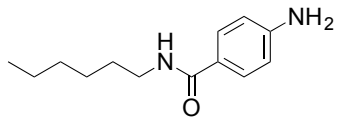


A solution of azide **4** (200 mg, 0.81 mmol) and 10% Pd/C (20 mg, 0.19 mmol) in MeOH (5 mL) was stirred at RT under a $H_2$ (1 atm) atmosphere for 3 h. After this time, the mixture was filtered through Celite®. Then, the mixture was concentrated under reduced pressure to yield amine **5** as an amorphous beige solid (168 mg, 95%). Mp: 102-104 °C. $\nu_{max}$ (ATR): 3410 (NH), 3329 (NH), 3215 (CH), 2955 (CH), 2924 (CH), 2855 (CH), 1637 (C=O), 1601 (Ar), 1537 (Ar), 1504 (Ar). $\delta_H$ ($CDCl_3$, 400 MHz): 7.58 (2H, d, $J$ = 8.6 Hz, H-2', H-6'), 6.60 (2H, d, $J$ = 8.6 Hz, H-3', H-5'), 6.26 (1H, broad s, NH), 4.05 (2H, s, $NH_2$) 3.45-3.41 (2H, m, $CH_2$-1]), 1.60 (2H, qn, $J$ = 7.0 Hz, $CH_2$-2), 1.40-1.28 (6H, m, $CH_2$-3, $CH_2$-4 and $CH_2$-5), 0.91-0.87 (3H, t, $J$ = 7.0 Hz, $CH_3$). $\delta_C$ ($CDCl_3$, 100 MHz): 166.57 (C), 152.43 (C), 133.65 (C), 128.88 (CH), 117.88 (CH), 40.27 ($CH_2$), 31.63 ($CH_2$), 29.75 ($CH_2$), 26.79 ($CH_2$), 22.67 ($CH_2$), 14.14 ($CH_3$). LRMS ($ESI^+$) 243 [$(M + Na)^+$, 100%] HRMS ($ESI^+$): 243.1469. $C_{13}H_{20}N_2ONa$ requires $(M + Na)^+$, 243.1468. IR data in broad agreement with Lit. [2].

**Supplementary References**

1. J. D. Knight, S. J. Sauer and D. M. Coltart, *Org. Lett.*, 2011, **13**, 3118-3121.
2. C. R. Clark, M. J. M. Wells, R. T. Sansom, G. N. Norris, R. C. Dockens and W. R. Ravis, *J. Med. Chem.*, 1984, **27**, 779-782.

# Assessment of $H_2S$ *in vivo* using the newly developed mitochondria-targeted mass spectrometry probe MitoA

Sabine Arndt, Carlos D. Baeza-Garza, Angela Logan, Tiziana Rosa, Rudolf Wedmann, Tracy A. Prime, Jack L. Martin, Kourosh Saeb-Parsy, Thomas Krieg, Milos R. Filipovic, Richard C. Hartley and Michael P. Murphy

*J. Biol. Chem. 2017, 292:7761-7773.*
*doi: 10.1074/jbc.M117.784678 originally published online March 20, 2017*

---